EXPERIMENTS AND THEORY ON FLOW IN THE DIFFUSER

YOSHIMASA FURUYA

Department of Mechanical Engineering

(Received May 31, 1958)

Nomenclature

x : distance from the diffuser entrance
y : distance from the wall
u : x component velocity in boundary layer
v : y component velocity
U : velocity outside the boundary layer
$\overline{U}$: cross-sectional mean velocity
u' : root mean square value of velocity fluctuation in x direction
q_s : dynamic pressure of surface pitot-tube
δ : boundary layer thickness
δ^* : displacement thickness
θ : momentum thickness
θ^* : energy thickness
$H=\delta^*/\theta$, $H^*=\theta^*/\theta$
$\kappa=(u/U)_{y=0}$
τ_0 : frictional stress on wall
$u_*=\sqrt{\tau_0/\rho}$, $C_f=\tau_0\Big/\frac{\rho}{2}U^2$
p : pressure
h, b: height and width of rectangular cross-section respectively
r : inner radius of pipe
l : mixing length, length of approach pipe
A : cross-sectional area
$R_\theta=U\theta/\nu$, $R_x=Ux/\nu$
$\zeta=(\tau_0/\rho U^2)R_\theta^{1/4}$, $\Gamma=-(\theta/\rho U^2)R_\theta^{-1/4}dp/dx$
X= inertia term in Eq. (4.23)

Introduction

The diffuser is used to convert high velocity energy into pressure energy, as, for instance, in pipes discharging fluid from turbines, pump and blower.

The energy loss in the diffuser is often the greatest loss in the fluid mechanical machines equiped with a diffuser and depends on the behavior of boundary layer flow which is generally in the state of turbulent in as much as the flow becomes separate from the wall through adverse pressure gradient.

Contributions to experimental data on the energy loss in the diffuser and on flow in the diffuser are Gibson,[1] Andres,[2] Lyons,[3] Peters,[4] Vüller,[5] Shogenji,[6] Fujimoto[7] and others who describe either the energy loss in the diffuser or the pressure recovery performance of the diffuser for various diffuser forms and for various angle of diffusers. Hochschild,[8] Kröner,[9] Dönch,[10] Nikuradse[11] described velocity distributions in some types of diffusers and Nikuradse described a condition for flow separation in some types.

We used some of these experimental results when we designed a diffuser for the purpose of estimating the energy loss. It is not possible, however, to apply the data for one diffuser to a proposed diffuser unless the condition of the latter is much the same as that of the former.

On the other hand, investigations of the behavior of turbulent boundary layers have been conspicuous and a number of empirical formulae have been suggested within the last fifteen years. Gruschwitz,[12] Buri,[13] Kehl,[14] Doenhoff and Tetervin,[15] Garner,[16] Rotta,[17] Truckenbrodt,[18] Fujimoto,[19] Schuh[20] present semi-empirical formulae for calculating turbulent boundary layers under the influence of adverse pressure gradient.

These formulae may be helpful for diffuser flow, but they have proved unsatisfactory when the approach to the flow separation point is considered.

Thus a theoretical procedure for estimating the energy loss in the diffuser has not yet been established.

This paper is concerned with experiments and theory on flow in diffusers, especially on the condition of flow separation.

Chapter I. Boundary Layer Thicknesses and Diffuser Performances

1. Flow condition and diffuser form

Attention is directed in this paper to steady noncompressible flow in diffusers of simple form having smooth wall sufaces. In as much as the radius of curvature of flow stream-line is large as compared with the boundary layer thickness, excepting in the diffuser entrance, pressure can be considered constant within cross-sections of the diffuser.

We consider a diffuser having two-dimentional or circular or rectangular cross-sections with small diverging angles.

The diffuser boundary layer is usually considered to be in a turbulent state starting from the entrance of the diffuser. The flow outside the boundary layer consists of frictionless flow, the velocity of which can be assumed to be uniform within cross-sections of the diffuser excepting in the entrance. These assumptions can be used even for an extreme case where the boundary layer increases to the center line of the diffuser which occurs when the flow passes through a long pipe before approaching the diffuser.

In this paper we treat mainly with the two-dimentional diffuser but we also include flow in conical and rectangular diffuser which are not two-dimentional.

2. Relation between layer thickness and diffuser characteristics

To determine behavior of the flow in each cross-section of the diffuser as well as to note the flow separation, in our calculation we used characteristic thicknesses

of boundary layer and velocity outside the layer instead of cross-sectional mean velocity and mean energy which prevail in hydraulics.

The characteristic thicknesses of the boundary layer in two-dimentional diffuser and in conical diffuser respectively are defined by

δ^*: displacement thickness:

$$\int_0^\delta \left(1-\frac{u}{U}\right)dy \text{ (two-dimentional)} \quad \text{and} \quad \int_0^\delta \left(1-\frac{u}{U}\right)\frac{r}{r_0}dy \text{ (conical)} \tag{1.1}$$

θ: momentum thickness:

$$\int_0^\delta \frac{u}{U}\left(1-\frac{u}{U}\right)dy \quad \text{and} \quad \int_0^\delta \frac{u}{U}\left(1-\frac{u}{U}\right)\frac{r}{r_0}dy \tag{1.2}$$

θ^*: energy thickness:

$$\int_0^\delta \frac{u}{U}\left\{1-\left(\frac{u}{U}\right)^2\right\}dy \quad \text{and} \quad \int_0^\delta \frac{u}{U}\left\{1-\left(\frac{u}{U}\right)^2\right\}\frac{r}{r_0}dy \tag{1.3}$$

where u is velocity in the boundary layer, U velocity outside the layer, r_0 radius of circular cross-section of conical diffuser.

For symmetrical two-dimentional diffuser and conical diffuser respectively, the equation of continuity gives

$$\begin{aligned} &\text{total flow/unit width}: && \overline{U}h = Uh(1-2\delta^*/h) = \text{constant} \\ &\text{total flow}: && \overline{U}r_0^2 = Ur_0^2(1-2\delta^*/r_0) = \text{constant} \end{aligned} \tag{1.4}$$

where $\overline{U}$ is cross-sectional mean velocity and h is distance between two diverging walls in cross-sections of two-dimentional diffuser.

From Eq. (1.4), we get the relation between $\overline{U}$ and U and Bernouilli's equation holds in the potential flow outside the layer, *viz*,

$$p+\frac{\rho}{2}U^2 = \text{constant} \tag{1.5}$$

then pressure p along the flow can be determined by the displacement thickness.

By using momentum thickness (1.2), total momentum of flow at a cross-section can be expressed respectively for two-dimentional diffuser and for conical diffuser as

$$\begin{aligned} \int_A \rho u^2 dA &= \rho U^2 A\left(1-2\frac{\delta^*+\theta}{h}\right) \text{ (two-dimentional)} \\ \text{and} \quad &= \rho U^2 A\left(1-2\frac{\delta^*+\theta}{r_0}\right) \text{ (conical)} \end{aligned} \tag{1.6}$$

where A is cross-sectional area.

In the same manner, total kinetic energy of flow at a cross-section respectively of both these diffusers is

$$\int_A \frac{\rho}{2}u^3 dA = \frac{\rho}{2}U^3 A\left(1-2\frac{\delta^*+\theta^*}{h}\right) \quad \text{and} \quad = \frac{\rho U^3}{2}A\left(1-2\frac{\delta^*+\theta^*}{r_0}\right). \tag{1.7}$$

The loss of head between two cross-sections of the two-dimentional diffuser can be expressed by

$$(p_1/\gamma+\alpha_1\cdot\overline{U}_1^2/2g)-(p_2/\gamma+\alpha_2\cdot\overline{U}_2^2/2g) \tag{1.8}$$

where subscripts 1 and 2 designate characteristics in the initial cross-section and on the final cross-section respectively and the velocity profile coefficients α_1 and α_2 are defined by

$$\alpha_1=\int_{A_1}\frac{1}{2}\rho u^3dA\Big/\frac{1}{2}\rho\overline{U}_1^3A_1,\qquad \alpha_2=\int_{A_2}\frac{1}{2}\rho u^3dA\Big/\frac{1}{2}\rho\overline{U}_2^3A_2. \tag{1.9}$$

By the use of Eqs. (1.4) and (1.7), these coefficients are rewritten as follows:

$$\alpha_1=\left(1-2\frac{\delta_1^*+\theta_1^*}{h_1}\right)\Big/\left(1-2\frac{\delta_1^*}{h_1}\right)^3,\qquad \alpha_2=\left(1-2\frac{\delta_2^*+\theta_2^*}{h_2}\right)\Big/\left(1-2\frac{\delta_2^*}{h_2}\right)^3 \tag{1.10}$$

Eqs. (1.8), (1.10) also be used for the conical diffuser when radius r_0 is used instead of distance h, as in Eqs. given below.

Following Peters,[3)21)] the diffuser efficiency of pressure recovery η is defined by

$$\eta=\frac{(p_2-p_1)\overline{U}A}{\int_{A_1}\frac{1}{2}\rho u^3dA-\int_{A_2}\frac{1}{2}\rho u^3dA}. \tag{1.11}$$

From Eqs. (1.4) and (1.5), we obtain

$$p_2-p_1=\frac{\rho}{2}\overline{U}_1^2\left\{\frac{1}{\left(1-2\frac{\delta_1^*}{h_1}\right)^2}-\left(\frac{h_1}{h_2}\right)^2\frac{1}{\left(1-2\frac{\delta_2^*}{h_2}\right)^2}\right\}. \tag{1.12}$$

By the use of Eqs. (1.9) and (1.12), Eq. (1.11) is rewritten as

$$\eta=\left\{\frac{1}{\left(1-2\frac{\delta_1^*}{h_1}\right)^2}-\left(\frac{h_1}{h_2}\right)^2\frac{1}{\left(1-2\frac{\delta_2^*}{h_2}\right)^2}\right\}\Big/\left\{\alpha_1-\alpha_2\left(\frac{h_1}{h_2}\right)^2\right\}. \tag{1.13}$$

As shown in these equations, diffuser performance can be determined by the characteristic thickness of the boundary layer. In these calculations, we assumed the flow to be symmetrical about the center axis of the diffuser. When the flow separates from the wall, however, it is no longer symmetrical[11)] and the above equations can not hold after flow separation.

3. Relations of boundary layer thicknesses

As shown in the previous section, characteristic thicknesses of boundary layer are determined by the velocity profile in the boundary layer. It is found that all velocity profiles in turbulent boundary layers when expressed in non-dimentional form as u/U versus y/θ are arranged as a single group of curves as will be explained in Chapter III. Therefore, when we take the ratio of these boundary layer thicknesses as $H=\delta^*/\theta$, $H^*=\theta^*/\theta$, two parameters H and H^* can be determined in a fixed relation.

The experimental values of H^* are plotted against the values of H in Fig. 1.1 where the dotted line shows a empirical formula by others.[22)] Here, the full line shows the result of calculations in which it is assumed that the velocity profile in

the boundary layer can be expressed by a power relation of the form

$$u/U=(y/\delta)^n \qquad \text{resulting in}$$
$$H^*=4H/(3H-1). \qquad (1.14)$$

As shown in Fig. 1.1, the value of H^* is determined by the value of H.

From these fact, we can conclude that the diffuser performance is determined by one thickness of the layers and one parameter H or by two thicknesses θ and δ^*.

Because momentum thickness θ can be determined theoretically by the momentum equation of the form[23]

$$\frac{d\theta}{dx}=\frac{\tau_0}{\rho U^2}-(H+2)\frac{\theta}{U}\frac{dU}{dx}$$

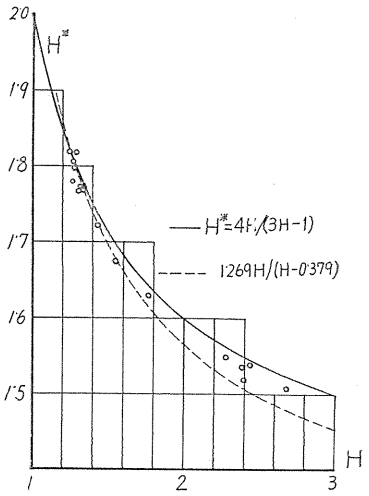

FIG. 1.1

where τ_0 is friction stress of flow on the wall, then the theories for parameter H (or for displacement thickness δ^*) and for friction τ_0 are needed in order to calculate flow in and performance of the diffuser.

Chapter II. Experimental Equipment and Techniques

1. Equipment for measuring velocity profile in boundary layer

As the velocity distribution in boundary layer of diffuser can not be determined theoretically, we can decide it only by experiment. Here we carry out experiments on velocity distribution and on shearing stress in the diffuser.

Fig. 2.1 is the schematic arrangement of equipment used in this experiment. This test diffuser consists of four smooth brass plates, two placed parallel vertically to form the side walls, the other horizontally at a divergent angle to form the top and lower wall, making a rectangular section. Measurements are carried out on the lower wall along the center line where the flow is nearly two-dimentional. Two-dimentionality of the flow will be discussed later in Chapter V under the "Effect of aspect ratio of rectangular diffuser on two-dimentionality of flow."

Range of thickness of boundary layer δ is from 8 mm to 50 mm ($U\delta/\nu=2\times10^4 \sim 1.3\times10^5$). Mean velocity is measured with a pitot-tube which has an opening of 0.6 mm and can be moved by micrometer giving accuracy of 0.02 mm. Pressure along the flow is controlled by form and position of upper wall, as shown in Fig. 2.2 where No. in each test diffuser refers to No. of test.

To prevent separation of flow at the upper wall and to get greater pressure gradient, the boundary layer flow on upper wall is forced to go out through slits in the wall (No. 8 in Fig. 2.2). To increase boundary layer, an approach leading to the diffuser is partially covered by a corrugated plate laid 155 mm away from inlet section (test No. 9-10 in Fig. 2.2).

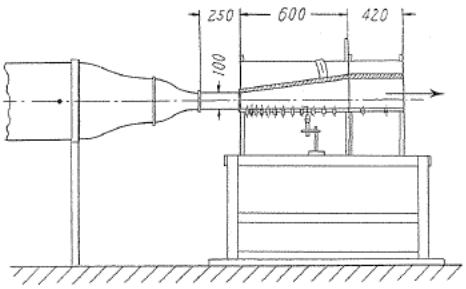

FIG. 2.1

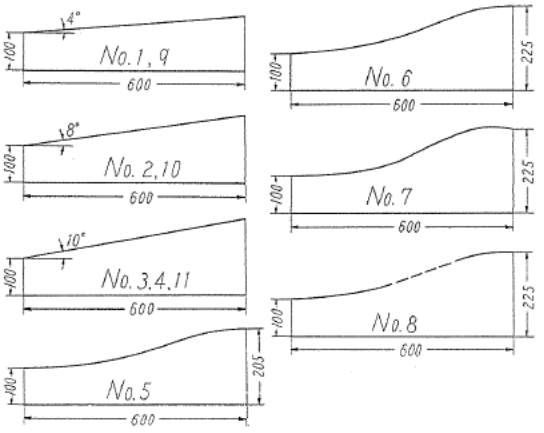

FIG. 2.2

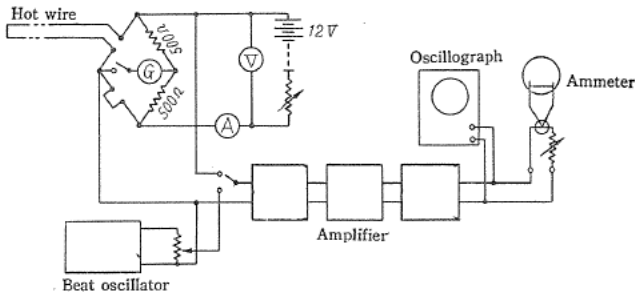

FIG. 2.3

To measure fluctuation of velocity in the boundary layer, a platinium hot-wire anemometer is used. Anemometer arrangement is shown in Fig. 2.3. To compensate for thermal lag on the hot-wire, a C-R coupling amplifier is used whereby the time constant ($M = CR$) can be conveniently changed by changing the capacity in the amplifier.

The time constant is calibrated by using square wave electric current to heat the wire.

2. Equipment for measuring shearing stress[24]

To obtain detailed information on flow in turbulent boundary layer, it is necessary to know the amount of surface friction on the wall.

To measure surface friction, surface pitot-tube of Stanton type[25] is used, but measuring with the surface-tube presents some experimental difficulties; for instance, the uncertaincy of measurement and the effect of pressure gradient of flow on the measurement. Neither of these difficulties have yet been resolved.

Our experimental program is initiated to clarify these difficulties by finding the characteristics of the surface-tube.

The surface-tube and test channel used for one of these calibrations are pictured in Fig. 2.4 where dimentions of channel and tube are given. Flow in the channel is two-dimentional laminar flow. A smooth brass circular tube of 29.1 mm diameter is also used to calibrate the same tube. Flow in the pipe is turbulent.

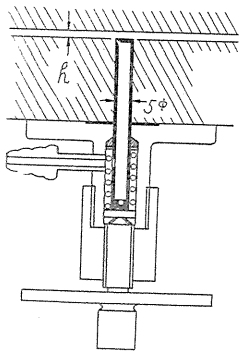

Channel

Clearance h	Breadth	Length
0.72 mm	50 mm	450 mm
1.07 〃		
1.6 〃		
2.1 〃		

FIG. 2.4

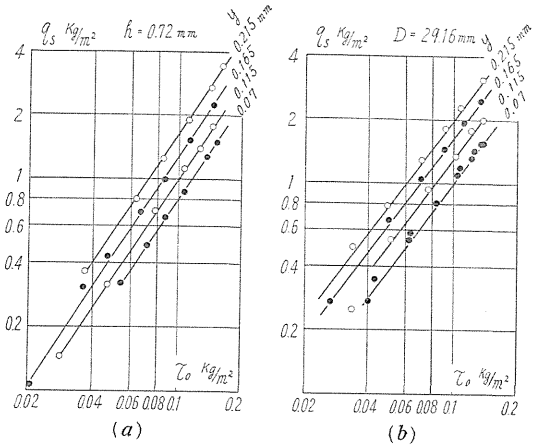

FIG. 2.5

Measurements are made by changing both air velocity and tube opening to obtain both shearing stress of flow on the wall τ_0 and dynamic pressure in the surface-tube q_s. These results are shown in Fig. 2.5 (a), (b). Fig. 2.5 (a) shows calibration of the tube in laminar flow and Fig. 2.5 (b) calibration of the same tube in turbulent flow. Both calibration curves are nearly the same and can be expressed by

$$q_s \infty \tau_0^n \tag{2.1}$$

where n changes from 1.36 to 1.5 depending upon the tube opening.

We tested the effect of pressure gradient by changing clearance between two walls of channel as in Fig. 2.4, because positive pressure gradient dp/dx along the flow is in inverse proportion to the clearance of the channel h as expressed by

$$1/\tau_0 \cdot dp/dx = -2/h. \tag{2.2}$$

The results are shown in Fig. 2.6 where the different symbols refer to different clearance. As seen here, the effect of pressure gradient is not easily recognized as being within the error of the measurement. Because the condition of tube opening is not exactly the same in each test after readjusting the tube, we found that the condition is responsible for the error.

Another type of surface tube is made by placing a small (10 mm × 13 mm) thin (0.75 mm thick) steel plate having one sharp edge fixed on the center line of test wall. As shown on Fig. 2.7, the effect of pressure gradient still can not be recognized although the error of measurement is decreased. After several testing, a plate having an opening of 0.175 mm was found to be most convenient and efficient for measuring shearing stress in diffuser experiments.

When the plate is fixed on the test diffuser wall, as shown in Fig. 2.8, dynamic pressure in the tube is calibrated by wall shearing force which is derived from change of momentum thickness along the flow by keeping constant pressure along

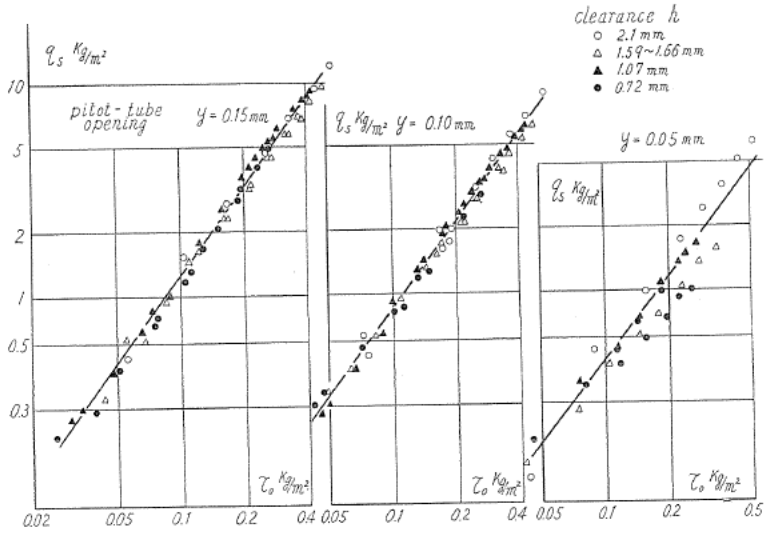

FIG. 2.6

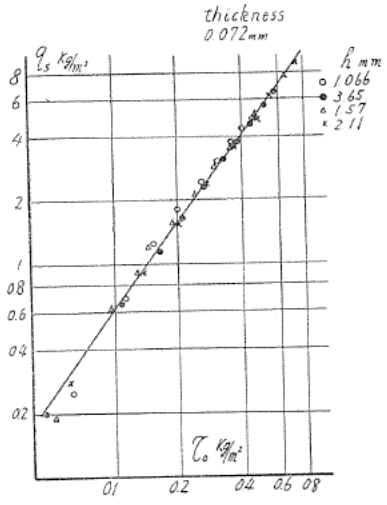

FIG. 2.7

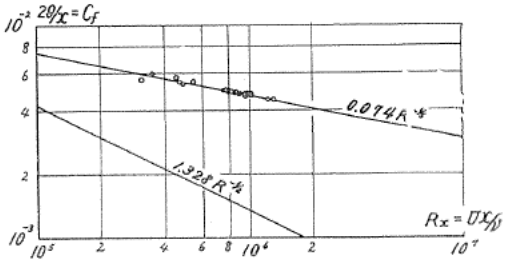

FIG. 2.9

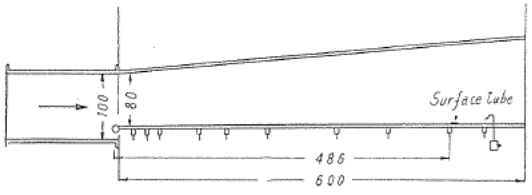

FIG. 2.8

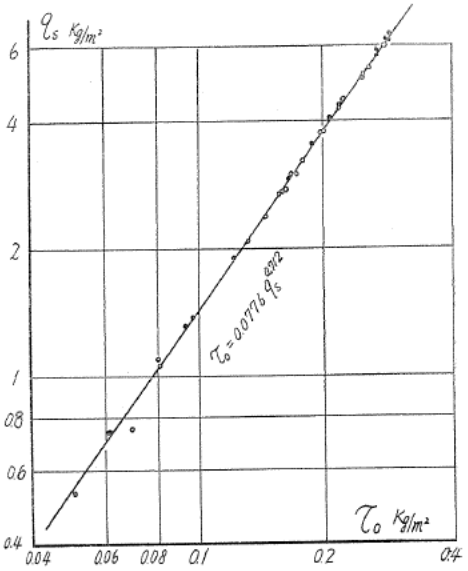

FIG. 2.10

the flow (Fig. 2.9). This result shows (Fig. 2.10) that

$$\tau_0 = 0.0776\, q_s^{0.712} \tag{2.3}$$

which is nearly equal to the result for the same opening condition in Fig. 2.5.

Chapter III. Results of Experiments

1. Velocity profile in turbulent boundary layer in diffuser[26]

In the test diffuser described in Fig. 2.2, we measure the pressure distribution along the flow. The results are shown in Fig. 3.1 (a), (b) where the dynamic pressure of potential flow in any section $\frac{1}{2}\rho U^2$ devided by that in the inlet section $\frac{1}{2}\rho U_1^2$, is shown against x (x: distance from the inlet section).

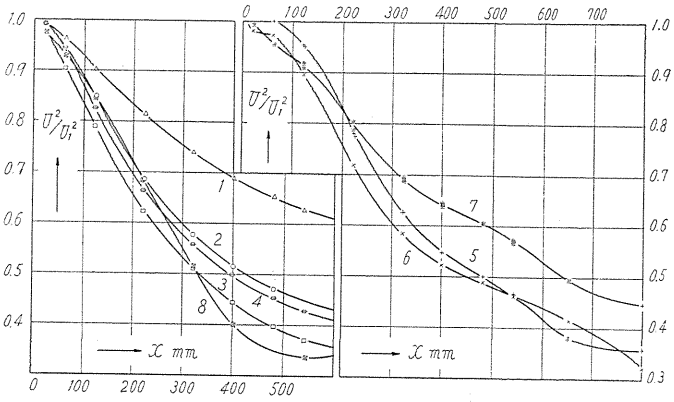

FIG. 3.1 (a)

The velocity curves in the turbulent boundary layer in these pressure distributions are shown in Fig. 3.2 (a), (b) where the velocity ratio u/U is shown against $\log y$ (y: distance from the wall, U: velocity outside the boundary layer).

When the velocity curves are expressed in non-dimentional form u/U versus y/θ (θ: momentum thickness), as shown in Fig. 3.3, all velocity curves are, on the whole, found to be regularly arranged in single group of curves, as described by Gruschwitz[12] and others.[15]

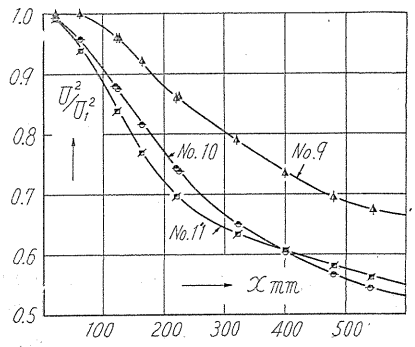

FIG. 3.1 (b)

There is, however, a slight irregularity in arrangement of curves near the wall. The velocity ratio u/U in the downstream part of the diffuser, *i.e.* in high Reynolds number, is slightly larger than that in the upstream part, *i.e.* than in lower Reynolds number. An example of the difference in curves caused b by Reynolds number is shown in Fig. 3.4.

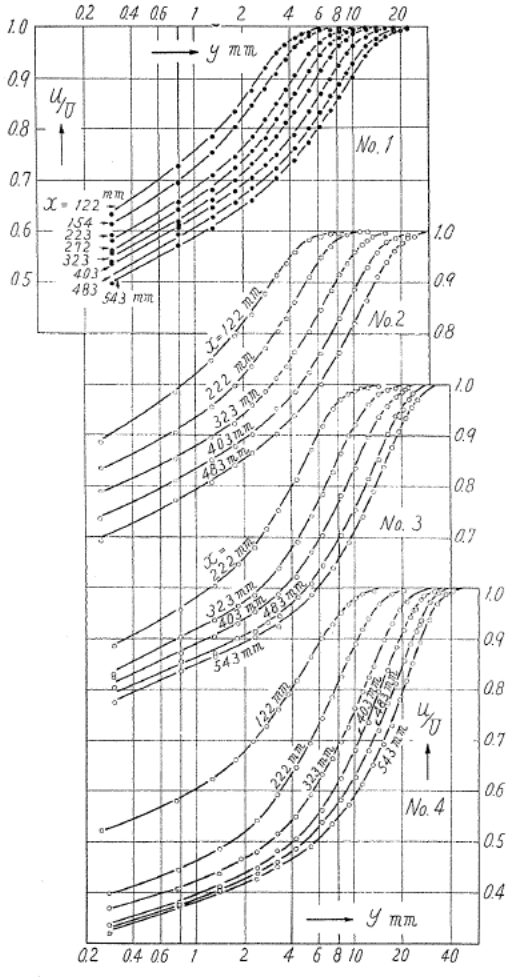

FIG. 3.2 (*a*)

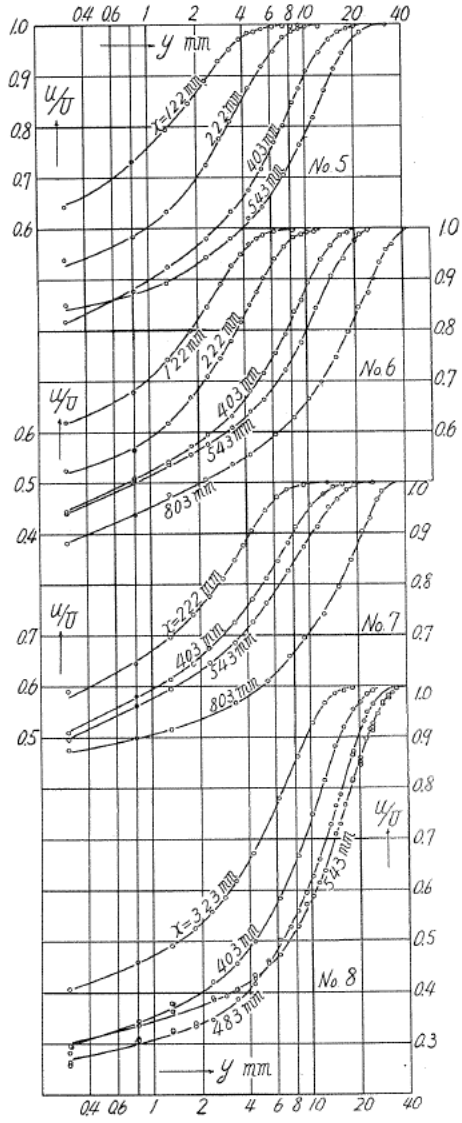

FIG. 3.2 (*b*)

Comparing our result on velocity curves with those of Nikuradse[11] and Gruschwitz,[12] agreement is good on the whole being within an error of 2–3%, and we found a slight irregularity near the wall on curves of lower Reynolds number in Gruschwitz experiments (Fig. 3.5).

Fig. 3.6 shows the value of u/U at $y=\theta$ (later denoted as κ) against the value of the parameter of velocity curve $H=\delta^*/\theta$. Here plots of our experiments and those of Nikuradse are given in a single curve. From this we found that velocity curves in the diffuser within some range of Reynolds number are decided by a single parameter H or κ,

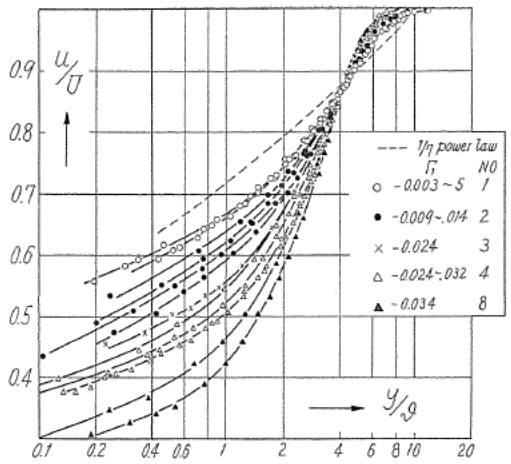

FIG. 3.3 (*a*)

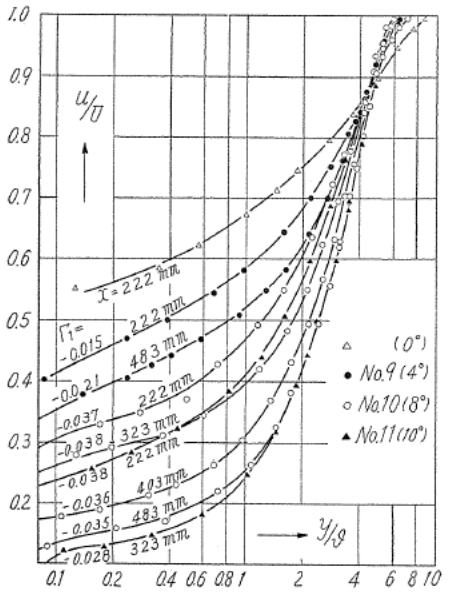

FIG. 3.3 (*b*)

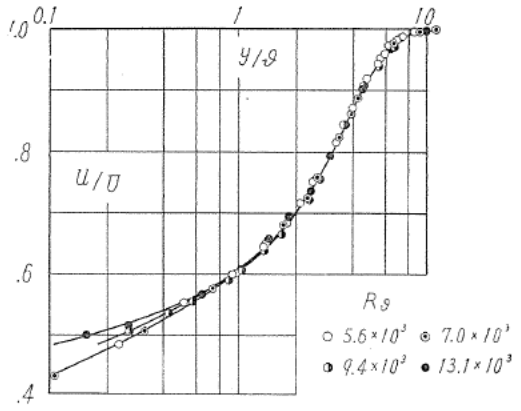

FIG. 3.4

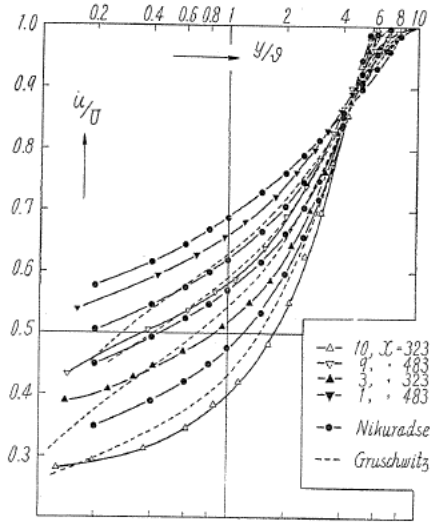

FIG. 3.5

Next, we examine the relation between the form parameter H in any corss-section and Buri's[13] non-dimentional pressure gradient $\Gamma = -\theta R_\theta^{1/4} \frac{1}{\rho U^2} \frac{dp}{dx}$ at the same point. While some relation might be anticipated, our results indicates that there is no direct relation between H and Γ as shown in Fig. 3.7.

Using the mixing length of Prandtl[27] is a convenient way to trace velocity distribution in boundary layer. By plotting the curves of total head versus x along

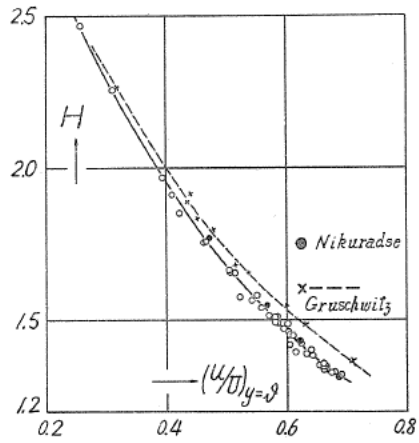

FIG. 3.6

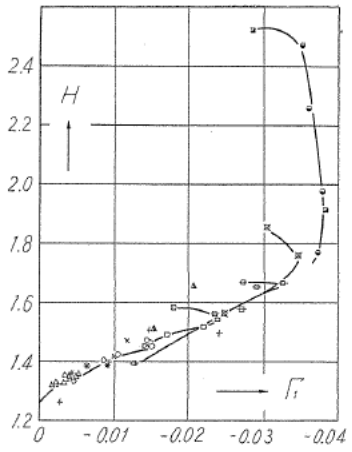

FIG. 3.7

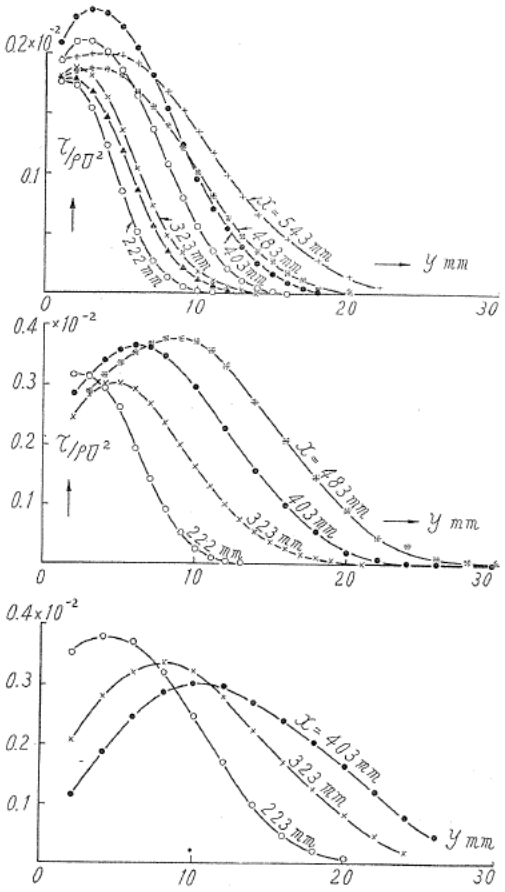

FIG. 3.8

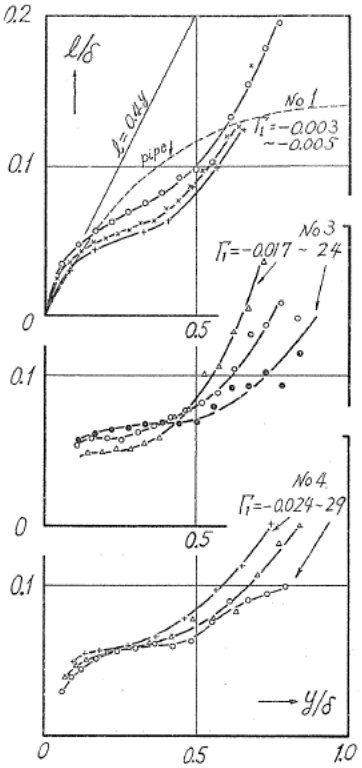

FIG. 3.9

the flow for each stream-line, and by finding the rate of change of total head along the flow, and by calculating the shearing stress distribution at several points (Fig. 3.8), we obtain the mixing length distribution from the shearing stress and the velocity distribution. The results are given in Fig. 3.9.

Here the curve of the mixing length tends to flatten as the pressure gradient becomes steeper, but the curve nearest the wall is found to remain nearly constant.

2. Velocity fluctuation in boundary layer

To properly discuss flow near the separation point, knowledge of velocity fluctuation in boundary layer is essential.

We measure velocity fluctuation along flow in boundary layer as the flow is approaching the separation point; turbulence intensity u' (u': intensity of velocity fluctuation in x direction) distribution in boundary layer is measured in a cross-section of the test diffuser by varying the diverging angles from 0 to 10 degree, with velocity remaining constant at the entrance (21 m/s). An example of measurements is given in Fig. 3.10. The relative values for turbulence u'/u and u'/U are shown in upper graph of Fig. 3.10. Time mean velocity u/U is given in lower graph of Fig. 3.10. As the diverging angle increases, or as the value of the parameter H increases, the value of relative turbulence u'/u near the wall increases greatly although the value of u'/U increases little. When the value of relative turbulence u'/u near the wall increases greater than 30-40%, where the flow is considered to have instantly reversed even though the flow in the time mean values has not yet reversed.

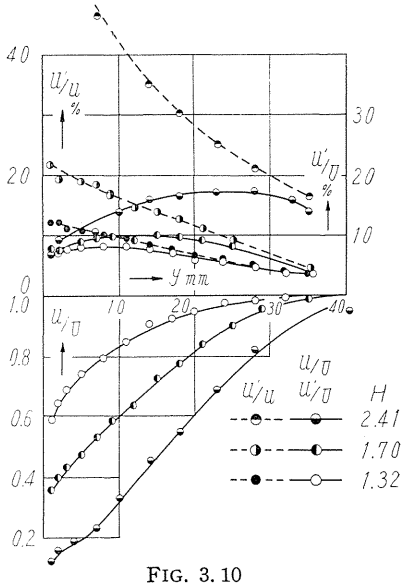

FIG. 3.10

Oscillographic records showing time mean variation of the velocity for 0, 4 and 8 degree of diverging angle in these experiments are given in Fig. 3.11 showing that the degree and mode of velocity fluctuation vary gradually untill the instant the reverse flow occurs.

Since the point of instant reverse flow is before the point where time-mean reverse flow occurs, the writer calls the condition of the former "Initial state of separation."

3. Wall friction and universal velocity distribution[24]

Ludwieg and Tillmann[28] and also Sandborn[29] measured wall friction of flow indirectly by heat transference from the wall. These results are applicable to diffuser flow except for flow near the separation point. On the other hand, it is said that parameter H of velocity profile at the separation point is 1.8 to 2.8, but there are no exact experimental results to decide this value.

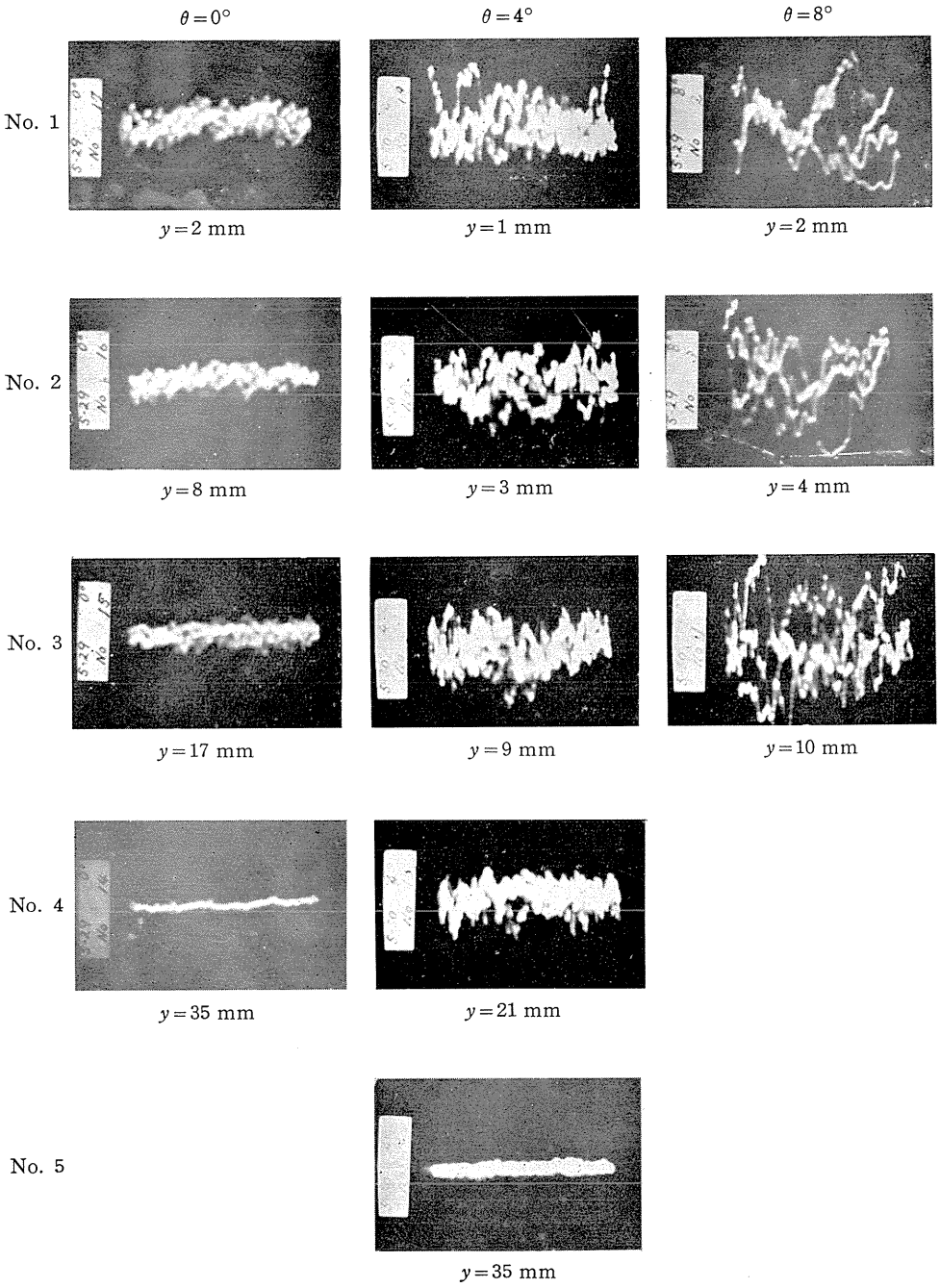

Time interval: 1/20 sec.
θ: Diverging angle.
y: Distance from the surface.

FIG. 3.11

We measured wall friction of diffuser flow by using the surface pitot-tube mentioned in Chapter II. 2. Results of our experiments are shown in Fig. 3.12 where the coefficient of wall friction $\zeta = (\tau_0/\rho U^2) R_\theta^{1/4}$ is plotted against the form parameter H.

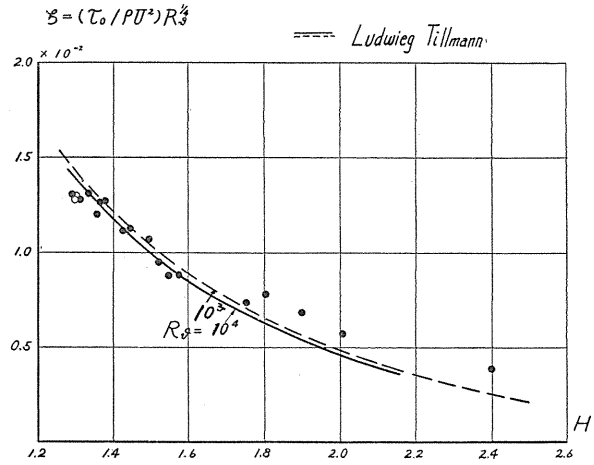

FIG. 3.12

Comparing these values with the formula of Ludwieg-Tillmann,[28]

$$\tau_0 \Big/ \left(\frac{1}{2}\rho U^2\right) = 0.246 \times 10^{-0.678H} R_\theta^{-0.268} \tag{3.1}$$

we know that as a whole the agreement is good, but when the parameter H is greater than 1.8, the values of ζ in our experiments are somewhat larger than those of the L-T formula.

Here we will discuss velocity distribution in the form u/u_* versus $u_* y/\nu$ where $u_* = \sqrt{\tau_0/\rho}$ is shearing velocity derived from results of wall friction. By using experimental results of wall friction, velocity distribution in boundary layer can be expressed in the form: u/u_* *vs.* $u_* y/\nu$.

Because wall friction and velocity are both measured in the same way with the pitot-tube, error of measurement will be canceled out in the ratio of u/u_*.

Our results are shown in Figs. 3.13, 14, 15. Fig. 3.13 shows that the velocity distributions in boundary layer with no pressure gradient have universal form regardless of Reynolds number. Fig. 3.14 shows that the velocity profile changes as the diverging angle increases but regardless of the diverging angle, the form near the wall does not change and can be expressed by

$$u/u_* = 4.4 + 5.75 \log_{10} (u_* y/\nu). \tag{3.2}$$

However, in Fig. 3.15 we see that when the adverse pressure gradient $-\Gamma$ increases further and the value of parameter H increases to greater than 1.8, the velocity form cannot hold the above equation even near the wall. The condition in which the velocity distribution near the wall cannot hold Eq. (3.2), is found to be nearly

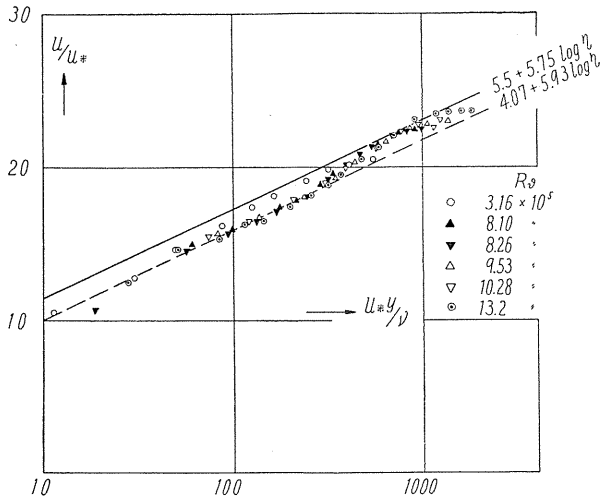

FIG. 3.13

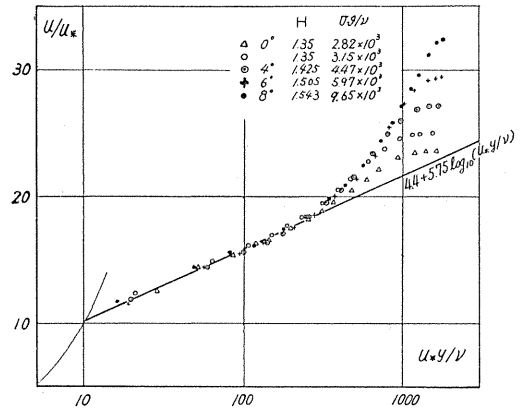

FIG. 3.14

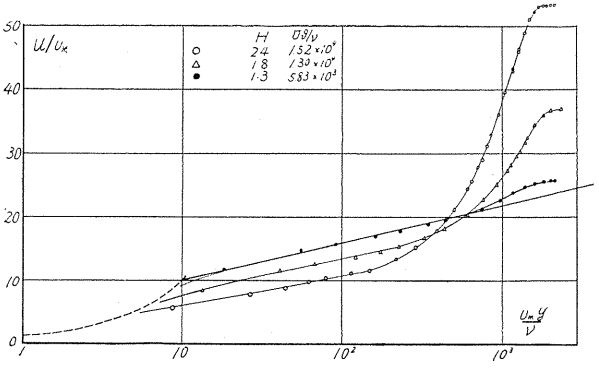

FIG. 3.15

the same as that of initial state of flow separation described in III. 2. Then we know that the initial flow separation occurs when $H \fallingdotseq 1.8$.

The value of this condition ($H=1.8$) is condiderably smaller than that of complete flow separation were H is 2.4-2.8.

Chapter IV. Empirical Formulae and Theories[30]

1. Empirical formulae for velocity profile near the wall of diffuser

As mentioned in Chapter III, all velocity profiles near the wall in diffusers when expressed in non-dimentional form u/u_* *vs.* u_*y/ν, *i.e.* wall-law, irrespective of pressure gradient, are practically the same except near the separation point and are expressed by

$$u/u_* = a_0 + a_1 \log_{10} (u_*y/\nu). \tag{4.1}$$

The values of these coefficients a_0 and a_1 determined by our experiments are shown in Table 4.1 and compared with values obtained by others for various turbulent boundary layers.

TABLE 4.1

a_0	a_1	Author	Condition of experiment
4.40	5.75	Present author Eq. (3.2)	Diffuser flow
4.90	5.60	Clauser[31]	Two-dimentional boundary layer with adverse pressure gradient
5.1	5.75	Coles[32]	〃
4.07	5.93	Schultz-Grunow[33]	Two-dimentional boundary layer without pressure gradient
5.5 5.57	5.75 5.87	Prandtl[34]	Pipe flow

As seen here, the values in our diffuser are nearly the same as those in other turbulent boundary layers.

We can substitute for Eq. (4.1) the approximation

$$u/u_* = \alpha(u_*y/\nu)^n \tag{4.2}$$

where the values α and n are obtained from Eqs. (4.1), (4.2) and are constant only within some range of Reynolds number u_*y/ν as shown in Fig. 4.1. When the Reynolds number u_*y/ν is smaller than 200, the values of α and n are 8.26 and 1/7 respectively and using these values, the velocity profile near the wall is satisfactorily expressed by Eq. (4.2) as shown in Fig. 4.2.

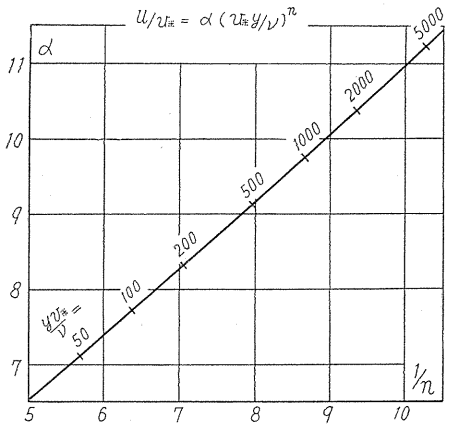

FIG. 4.1

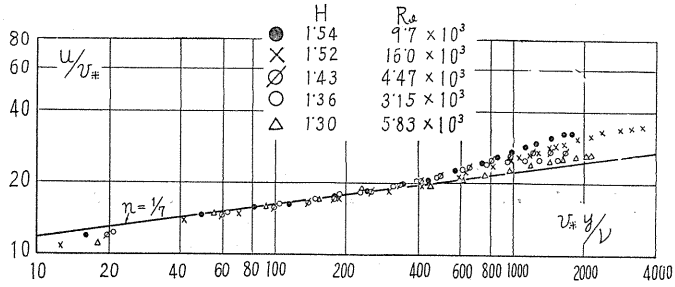

FIG. 4.2

As the momentum thickness θ is 1/10-2/10 of the whole thickness of the layer, we can assume that Eqs. (4.1) and (4.2) hold in the value of y ranging from the outside of laminar sublayer to the momentum thickness. Thus, rewriting Eq. (4.2) to get the relation between u/U and y/θ, we obtain the empirical formula for velocity profile near the wall

$$u/U=\kappa(y/\theta)^n \tag{4.3}$$

where κ denote the value of u/U at the point $y=\theta$ and is suitable parameter for shape of the velocity profile.

The relation between Gruschwitz's parameter[12] η_G and our parameter κ is expressed by $\eta_G=1-\kappa^2$.

2. Parameter for the shape of velocity profile

In this paper we use the value $\kappa=(u/U)_{y=0}$ as the parameter for velocity profile because this value can be determined by experiments on velocity profile in spite of the unfavorable condition that the value changes very slowly with Reynolds number even when the pressure along the flow is constant.

We calculate the value of the parameter when the pressure is constant. It is well known that the velocity profile in the boundary layer along the plate, or pipe, can be expressed by a relationship known as the velocity defect law:[33)35)]

$$(U-u)/u_*=f(y/\delta) \tag{4.4}$$

and that, excepting for the outer portion of the layer, the function f of Eq. (4.4) can be expressed as follows:

$$f=a_1\log_{10}(\delta/y)+b_0 \tag{4.5}$$

where the value of b_0 is 2.3-2.4.

From Eqs. (4.3), (4.4) and (4.5), we get the value of parameter in constant pressure κ_0 as follows:

$$\kappa_0=1-\frac{u_*}{U}[-a_1\log_{10}\{I_1\cdot(u_*/U)-I_2\cdot(u_*/U)^2\}+b_0] \tag{4.6}$$

where

$$I_1=\int_0^1 f d(y/\delta),\qquad I_2=\int_0^1 f^2 d(y/\delta) \tag{4.7}$$

and the value of I_1 and I_2 are respectively $I_1 = 3.33$, $I_2 = 20.3$.

As shown in Eq. (4.6), the value of κ_0 varies slightly with the value of $u^*/U = \sqrt{\tau_0/\rho U^2}$. There are many well-known relations between the friction coefficients u^*/U and Reynolds number $R_0 = U\theta/\nu$, one of which is expressed as follows:

$$U/u_* = 5.45 \log_{10} R_0 + 5.55. \quad (4.8)$$

From Eqs. (4.6), (4.8) we get a relationship between the parameters κ_0 and R_0 as shown in Fig. 4.3.

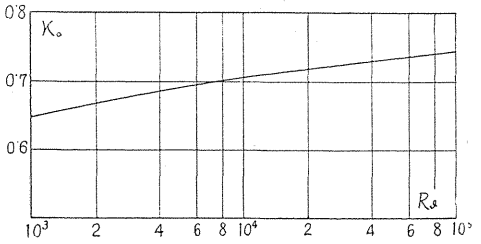

FIG. 4.3

The quantity $H = \delta^*/\theta$ is usually used instead of κ as the parameter for the velocity profile.

In order to find the relation between parameters κ and H in constant pressure, we rewrite Eq. (4.7) and get

$$H_0 = 1\Big/\left\{1 - \left(\frac{I_2}{I_1}\right) \cdot \frac{u_*}{U}\right\} \quad (4.9)$$

where H_0 is parameter H in constant pressure. Eliminating u_*/U from Eqs. (4.9), (4.6), we get

$$\kappa_0 = 1 - \frac{H_0 - 1}{G \cdot H_0}\left[-a_1 \log_{10}\{I_1 \cdot (H_0 - 1)/G \cdot H_0^2\} + b_0\right] \quad (4.10)$$

where $G = I_2/I_1 = 6.09$.

When the pressure gradient is adverse, the relation between parameter κ and parameter H can be obtained by the same procedure as used in Eq. (4.10) and is expressed by

$$\kappa = 1 - \frac{H - 1}{G \cdot H}\left[-a_1 \log_{10}\{I_1 \cdot (H - 1)/G \cdot H^2\} + b\right] \quad (4.11)$$

where the value of I_1, I_2, G and b vary according to pressure gradients. If we take the mean value of each constant as $I_1 = 6.29$, $b = 7.66$, $G = 10.05$, $a_1 = 5.6$, we get the equation

$$\kappa = 1 - 0.1\frac{H - 1}{H} \times [5.6 \log_{10}(H^2/H - 1) + 8.8]. \quad (4.12)$$

This relationship can be reduced to the following simple empirical equation:

$$H = 1.3 + 1.3(0.7 - \kappa) + 3(0.7 - \kappa)^2 \quad (4.13)$$

Fig. 4.4 shows Eq. (4.13) and experimental results.

The separation of flow occurs in the range of parameter H covering two-thirds

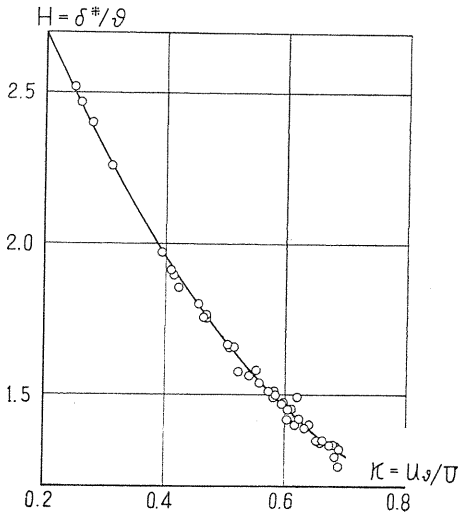

FIG. 4.4

(1.8–2.8) of the whole range (1.3–2.8) of the parameter, while the range of parameter κ in which the separation of flow occurs covers less than one-half (0.2–0.45) of the whole range of κ.

3. Shearing stress equation

From Eqs. (4.2) and (4.3) we get the equation of shearing stress at the wall $\tau_0/\rho U^2$ as follows:

$$\tau_0/\rho U^2 = \alpha^{-2/(n+1)} \cdot \kappa^{2/(n+1)} \cdot (U\theta/\nu)^{-2n/(n+1)}. \tag{4.14}$$

Using $n=1/7$, $\alpha=8.26$, from the above equation we have

$$\tau_0/\rho U^2 = 0.024\kappa^{1.75} R_\theta^{-0.25} \tag{4.15}$$

Eq. (4.15) is nearly the same as Ludwieg Tillmann's equation[28]

$$\tau_0 \Big/ \left(\frac{1}{2}\rho U^2\right) = 0.246 \times 10^{-0.678H} \cdot R_\theta^{-0.268}. \tag{4.16}$$

In as much as Eqs. (4.14) and (4.15) are reduced from the approximate equation (4.2), they can be used only for some range of Reynolds number. We consider the range of Reynolds number when pressure along the flow is constant.

When pressure along the flow is constant, parameter κ_0 is given in Fig. 4.3. Substituting κ_0 in Eq. (4.14) or Eq. (4.15), we get shearing stress as a function of R_θ which is shown in Fig. 4.5.

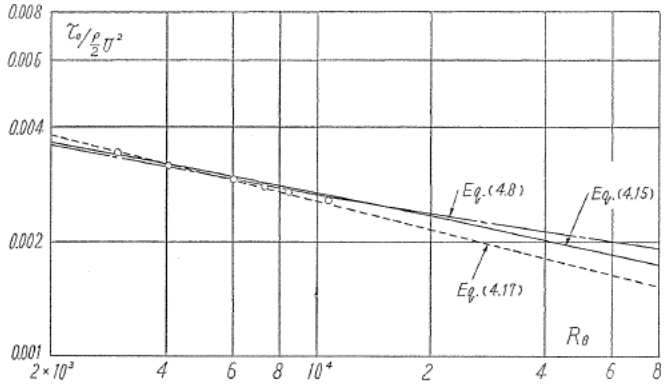

FIG. 4.5

So far, the Blasius's power equation[36] for shearing stress along the plate has been given as

$$\tau_0 \Big/ \left(\frac{\rho}{2} U^2\right) = 0.0256 R_\theta^{-1/4} \tag{4.17}$$

which is plotted by a broken line in Fig. 4.5.

From Fig. 4.5 we know that Eq. (4.15) can be used for a range of Reynolds number wider than can be used for Eq. (4.17).

When pressure along the flow has adverse pressure gradient, our experimental values of shearing stress are compared to values calculated from Eq. (4.15) as shown in Fig. 4.6. These results are in good agreement; there is only a slight difference near the separation point where H is larger than 1.8.

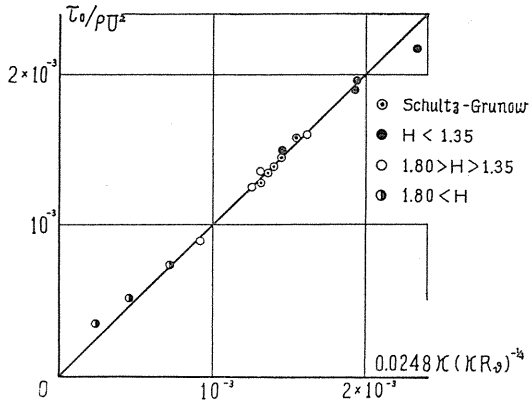

FIG. 4.6

Therefore Eq. (4.15) can be used for shearing stress in the diffuser except near the separation point.

4. Change of velocity profile equations

By using velocity profile equation (4.3) for the value of y ranging from the outside of laminar sublayer to the momentum thickness, we can derive equations of the rate of change of the parameter.

A two-dimentional equation of motion in boundary layer is

$$\rho u\partial u/\partial x+\rho v\partial u/\partial y=-dp/dx+\partial\tau/\partial y. \tag{4.18}$$

If the potential flow of velocity U exists outside the layer, we have

$$UdU/dx=-1/\rho\cdot dp/dx. \tag{4.19}$$

The equation of continuity is

$$\partial u/\partial x+\partial v/\partial y=0. \tag{4.20}$$

Substituting Eq. (4.3) into Eqs. (4.18), (4.19) and (4.20), we obtain

$$\frac{1}{(n+1)}\left(\frac{y}{\theta}\right)^{2n}\{\kappa\,d\kappa/dx+n\kappa^2/\theta\cdot d\theta/dx+\kappa^2/U\cdot dU/dx\}$$
$$=-1/\rho U^2\cdot dp/dx+1/\rho U^2\cdot\partial\tau/\partial y. \tag{4.21}$$

Integrating Eq. (4.21) with respect to y in the range from the outside of the sublayer y_0 to the momentum thickness θ, we get the momentum equation

$$\frac{\psi}{\tau}\{\theta\kappa\cdot d\kappa/dx-n\kappa^2\cdot d\kappa/dx+\theta\kappa^2/U\cdot dU/dx\}=-\frac{\theta}{\rho U^2}\frac{dp}{dx}+\frac{\theta}{\rho U^2}\frac{\tau_0-\tau_0}{\theta-y_0} \tag{4.22}$$

where

$$\gamma = \left(1 - \frac{y_0}{\theta}\right) \Big/ \{1 - (y_0/\theta)^{2n+1}\}$$

$$\psi = 1/(n+1)(2n+1).$$

Neglecting y, we get the following non-dimentional expression for Eq. (4.22)

$$X = (-\Gamma - Z)/\psi \tag{4.23}$$

where

$$X = -R_\theta^{2n/(n+1)}\theta\kappa\, d\kappa/dx + n\kappa^2 R_\theta^{2n/(n+1)}\, d\theta/dx - \theta R_0^{2n/(n+1)}\kappa^2/U \cdot dU/dx$$

$$\Gamma = \theta R_0^{2n/(n+1)}/U \cdot dU/dx$$

$$Z = \zeta(\tau_0 - \tau_0)/\tau_0 \qquad \zeta = (\tau_0/\rho U^2) R_0^{2n/(n+1)}.$$

This equation gives the linear relations between X and Γ.

The inclination of this relation is $(n+1)(2n+1)$ which is 1.469 for $n = 1/7$. The symbols X, Γ, Z are the inertia term, pressure term and friction term, respectively.

The value of Z depends on the shearing stress gradient near the wall: $(\partial\tau/\partial y)_{y=0} = dp/dx$. Therefore when $dp/dx = (\partial\tau/\partial y)_{y=0} = 0$, $Z = 0$ and when $dp/dx > 0$, $Z > 0$.

Fig. 4.7 shows the experimental results determined by Gruschwitz,[12] Doenhoff and Tetervin,[15] and Schubauer[39] as expressed in Eq. (4.23) where $n = 1/7$. Fig. 4.7 omits all their results in the range of $\kappa < 0.45$ *i.e.* all those near the separation point.

As shown in Fig. 4.7, all experimental results are distributed on the right-hand side along line $Z = 0$. The same experimental points are plotted in Fig. 4.8 where the expression $\theta R_0^{1/4} \cdot d\kappa/dx$,

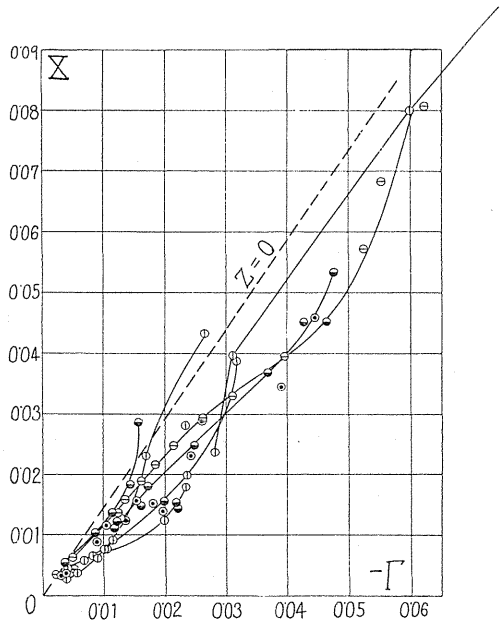

FIG. 4.7

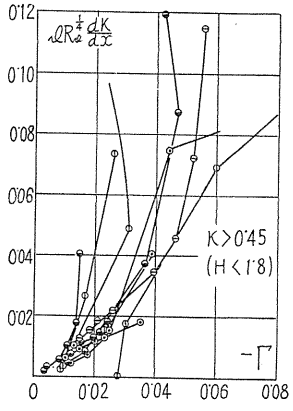

FIG. 4.8

vs. $-\Gamma$ is used. Comparing Fig. 4.7 with Fig. 4.8, we find that in the latter (Fig. 4.8) the experimental points are more scattered than in the former (Fig. 4.7). If we give the experimental data in still another expression as $\theta R_\theta^{1/4} dH/dx$, *vs.* $-\Gamma$, used more commonly than that in Fig. 4.8, the points are even more scattered.

One reason for this is that here (Fig. 4.8) the expression reveals unreliable data near the separation point.

According to Eq. (4.23), the value of shearing stress term can be determined by the horizontal distance between the experimental points and the line $Z=0$.

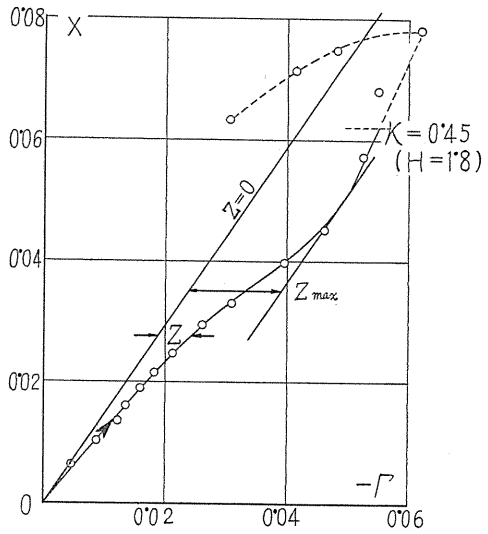

FIG. 4.9

As shown in Fig. 4.9, the values of Z increase with decrease of parameter κ until 0.45; apparently there is some relation between velocity profile and shearing stress distribution. However, value of κ under 0.45, there is no fixed relationship between the two parameters κ and Z.

In order to find the relationship between κ and Z for $\kappa > 0.45$, experimental data is plotted in Fig. 4.10.

The lines denoted by 1 show lines of constant values of Z corresponding to the fixed values of $\kappa = 0.65$, 0.60, 0.55, 0.50, 0.45. Line 2 shows the relationship between X and $-\Gamma$ when $d\kappa/dx = 0$, as derived from Karman's integral equation for momentum:

$$R_\theta^{1/4} d\theta/dx = -\Gamma(H+2) + \zeta. \tag{4.24}$$

Now we have the relation for the change of the parameter κ from which we can derive an empirical formula. From Eqs. (4.23) and (4.24) we obtain

$$\theta R_\theta^{1/4} \kappa\, d\kappa/dx = (\Gamma - \Gamma_0)\varphi \tag{4.25}$$

where

$$\varphi = -\frac{1}{\psi} - \kappa^2\{1 + n(H+2)\}$$

or

$$\varphi \fallingdotseq 1.46(1-\kappa^2) \quad \text{for} \quad n = 1/7$$

and

$$-\Gamma_0 = (Z/\psi + \zeta n\kappa^2)/\varphi.$$

By use of Fig. 4.10, the value of Γ_0 can be expressed as a function of parameter κ and we get the following equation:

$$\Gamma_0 = -0.118(0.67 - \kappa), \tag{4.26}$$

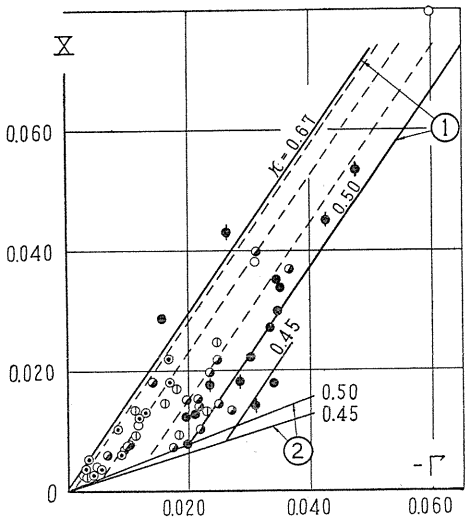

FIG. 4.10

Substituting Eq. (4.26) in Eq. (4.25), we have

$$\theta R_0^{1/4}\kappa\, d\kappa/dx = 1.46(1-\kappa^2)\{\Gamma - 0.118(0.67-\kappa)\}. \tag{4.27}$$

This equation holds for $\kappa > 0.45$, and because almost all experimental results show that the separation of flow occurs just after the value of κ decreases under 0.45 (Fig. 4.9), we assume the separation flow starts when $\kappa = 0.45$ ($H = 1.8$).

Eqs. (4.27) and (4.24) are two simultaneous first order differential equations which can be solved using the step-by-step method, giving θ and κ.

Eq. (4.26) of parameter κ can be transformed into an equation of parameter H by use of Eq. (4.13), and we have

$$\theta R_0^{1/4} dH/dx = -\alpha\Gamma - \beta \tag{4.28}$$

where constants α and β are functions of H (Fig. 4.11).

As already mentioned, there are several empirical equations which predict the behavior of boundary layers in adverse pressure gradient, the forms of which are approximately the same as in Eq. (4.28).

Recently Clauser[31] carried out experiments at Johns Hopkins University in which the velocity profiles were held constant; these results are shown in Fig. 4.12 where the non-dimentional pressure gradient $\theta/\tau_0 \cdot dp/dx$ is plotted against the form parameter H.

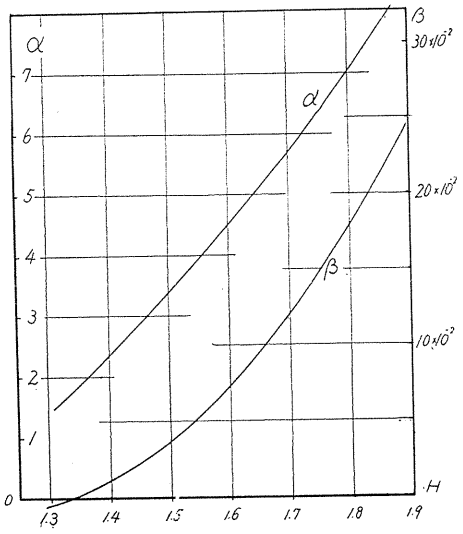

FIG. 4.11

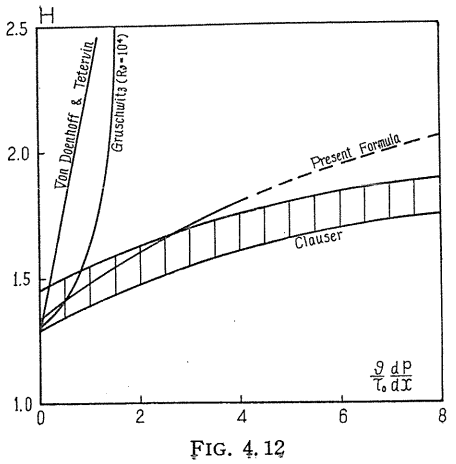

FIG. 4.12

Although these experimental results do not agree with that given by equation of Doenhoff and Tetervin[15] which was for several years the most representative of all equations, our formula introduced here shows far better coincidence.

5. Boundary layer equation for a circular and rectangular cross-sectional diffuser

So far our discussions have been mainly on equations of flow for only a two-dimentional diffuser. The forms of diffusers generally used are not only two-dimentional but have a circular or rectangular or other cross-section.

Here we first consider the flow in a diffuser having a circular cross-section.

Equation of motion for the boundary layer flow along the wall of this type diffuser is

$$ru\partial u/\partial x + rv\partial u/\partial y = -r/\rho \cdot dp/dx + 1/\rho \cdot \partial(r\tau)/\partial y \tag{4.29}$$

$$1/\rho \cdot \partial p/\partial x = -U \cdot dU/dx \tag{4.30}$$

and equation of continuity is

$$\partial(ur)/\partial x + \partial(vr)/\partial y = 0 \tag{4.31}$$

where r is distance from the center axis.

Integrating Eq. (4.29) by use of Eqs. (4.30) and (4.31), we get

$$\tau_0/\rho U^2 = 1/r_0 d(r_0\theta)/dx + (2+H)\theta/U \cdot dU/dx \tag{4.32}[38]$$

where r_0 is inner radius of wall

and
$$H = \delta^*/\theta \qquad \delta^* = \int_0^\delta \left(1 - \frac{u}{U}\right)\frac{r}{r_0}dy$$

$$\theta = \int_0^\delta \left(1 - \frac{u}{U}\right)\frac{u}{U}\frac{r}{r_0}dy.$$

Multiplying Eq. (4.29) by u and integrating it with respect to y from $y=0$ to $y=\delta$, we get

$$\frac{1}{r_0}\frac{d}{dx}(r_0\theta^* U^3) = \frac{2}{\rho}\int_0^\delta \tau \frac{\partial u}{\partial y}\frac{r}{r_0}dy \tag{4.33}$$

where

$$\theta^* = \int_0^\delta \frac{u}{U}\left[1 - \left(\frac{u}{U}\right)^2\right]\frac{r}{r_0}dy.$$

Substituting Eq. (4.32) in Eq. (4.33), we get

$$\theta\frac{dH^*}{dx} = H^*(H-1)\frac{\theta}{U}\frac{dU}{dx} + (2e - H^*)\frac{\tau_0}{\rho U^2} \tag{4.34}$$

where

$$H^* = \theta^*/\theta, \qquad e = \int_0^\delta \frac{\tau}{\tau_0}\frac{d(u/U)}{dy}\frac{r}{r_0}dy.$$

In Eq. (4.34), parameter H^* is determined by the value of parameter H because the velocity profile in the boundary layer can be determined single parameter H (see Chapter I).

In Eq. (4.34), shearing stress $\tau_0/\rho U^2$ is given in the form of

$$\tau_0/\rho U^2 = \xi(H) \cdot R_\theta^{-m} \tag{4.35}$$

which is determined by H and R_θ^{-m}.

The term of energy dissipation e in Eq. (4.34) is assumed to be expressed by

$$e = A(H) + \Gamma \cdot B(H) \tag{4.36}$$

where

$$\Gamma = \frac{\theta}{U}\frac{dU}{dx}R_\theta^m.$$

After substituting Eq. (4.35) and Eq. (4.36) in Eq. (4.34), we have

$$\theta R_\theta^m \frac{dH}{dx} = -\alpha(H) \cdot \Gamma - \beta(H) \tag{4.37}$$

where $\alpha(H)$ and $\beta(H)$ are functions of only H.

As Eq. (4.37) does not contain radius r_0, we may consider that it can be used regardless of the value of r_0 and can be used for two-dimentional flow ($r_0 = \infty$). Therefore the function α and β in Eq. (4.37) is the same as that of two-dimentional flow. Eqs. (4.32) and (4.37) are two simultaneous differential equations which can be solved by step-by-step method giving H and θ for the turbulent layer in the axially symmetrical diffuser.

Next, we consider the flow in the diffuser having a rectangular cross-section with constant width.

When the flow is not two-dimentional and diverges or converges as shown in Fig. 4.13, gradient of lateral velocity w in z direction (dw/dz) is not zero by using the coordinate as shown in Fig. 4.13. On the plane symmetry in this figure, equation of motion of boundary layer is

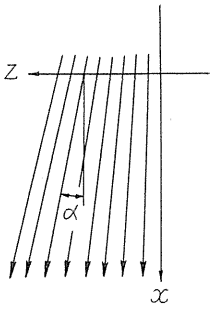

FIG. 4.13

$$u\frac{\partial u}{\partial x} + v\frac{\partial u}{\partial y} = -\frac{1}{\rho}\frac{\partial p}{\partial x} + \frac{1}{\rho}\frac{\partial \tau}{\partial y} \tag{4.38}$$

and equation of continuity is

$$\frac{\partial u}{\partial x} + \frac{\partial v}{\partial y} + \frac{\partial w}{\partial z} = 0. \tag{4.39}$$

Integrating Eq. (5.10) with respect to y, and eliminating v by the use of Eq. (5.11) and substituting $(d\alpha/dz)_{z=0} = \psi_0$, we get the following momentum equation:

$$\frac{d\theta}{dx} + \frac{\theta}{U}\frac{dU}{dx}(2+H) = \frac{\tau_0}{\rho U^2} - \psi_0\theta. \tag{4.40}$$

Comparing this equation with the two-dimentional equation, we find the additional term $-\psi_0\theta$ which has a considerable effect on $d\theta/dx$.

The equation of the change of parameter H for the rectangular diffuser can be derived by nearly the same procedure as that for getting Eq. (4.37) and the

equation thus obtained is the same as that for two-dimentional flow *i.e.* as in Eq. (4.37).

Therefore divergence or convergence of flow has no influence upon the equation of change of form parameter H.

By the use of Eqs. (4.40) and (4.37), the turbulent boundary layer in the rectangular diffuser can be calculated as giving H and θ when the pressure distribution along the flow in the diffuser is known.

6. Conclusion

By substituting the power formula for universal velocity distribution near the wall (wall law), the author advances a rational and simple method for estimating turbulent boundary layers in diffuser where the wall friction and velocity profile parameter are emphasized.

Light is thrown on the problem of turbulent boundary layers, revealing that other methods heretofore advanced are limited in use.

Chapter V. Effect of Aspect Ratio of Rectangular Diffuser on two-Dimentionality of flow

1. Introduction

The form and the thickness of the boundary layer of a diffuser determine its performance. Thickness of boundary layer in two-dimentional diffusers or axially symmetrical diffusers (conical type) can be estimated exactly by using the theory of two-dimentional boundary layer.

A diffuser of rectangular cross-section having two-parallel side walls is frequently used for a two-dimentional diffuser.

However, when the aspect ratio (distance between two parallel side walls/ distance between two divergent walls) of this rectangular section becomes small, the flow on the diverging wall is no longer two-dimentional and thus can not be exactly calculated by the two-dimentional theory, because in this case boundary layers on side walls can not be neglected.

2. Experiments on boundary layer thickness

Experiments[41] are carried out by this author and Y. Sugiyama to examine the effect of the aspect ratio on the two-dimentionality of boundary layer flow.

Arrangements of test diffuser are given in Fig. 5.1. Height of entrance (distance between two diverging walls) is 80 mm and width (distance between two side walls), which is constant for each diffuser type, varies according to type from 30 mm to 200 mm. Diverging angle may change from 4 to 8 degrees.

Special care is taken to secure uniform pressure distribution at the diffuser entrance. Straight pipe is used as an approach to the diffuser by which nearly constant pressure is obtained at the entrance; otherwise, pressure on the wall becomes considerably lower than pressure at the center. Pressure distribution along the flow is shown in Fig. 5.2 where chain lines give frictionless fluid when there is no boundary layer on the walls.

Velocity profiles in boundary layers are measured along the center line of the walls. The results are compared with the values calculared by two-dimentional equation. The dotted lines in Fig. 5.3 show the value of momentum thickness on

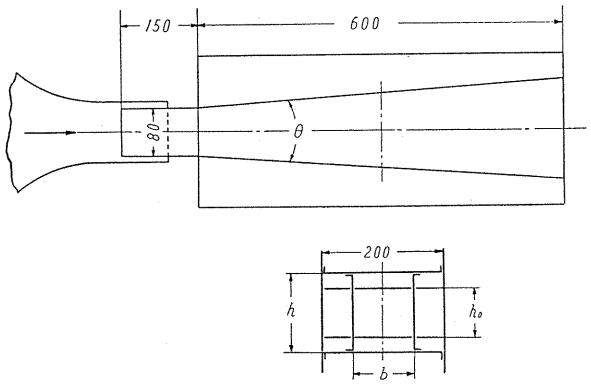

FIG. 5.1

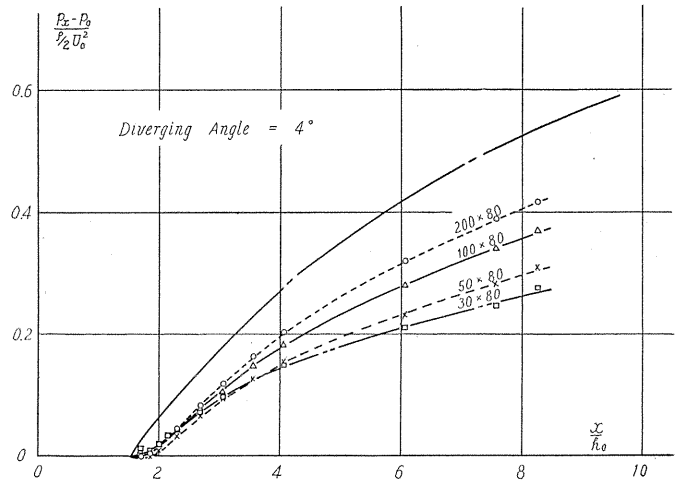

FIG. 5.2 (*a*)

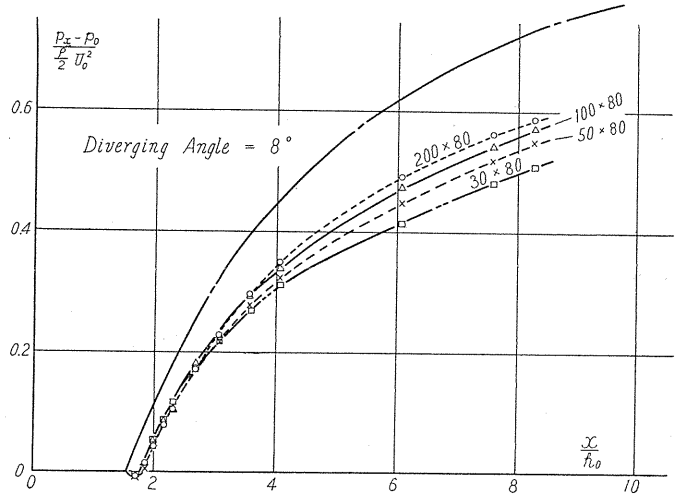

FIG. 5.2 (*b*)

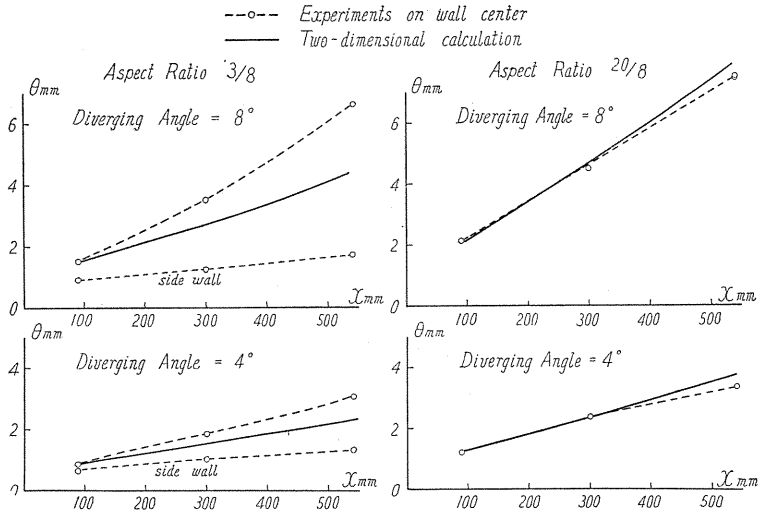

FIG. 5.3

wall center in test diffusers where, depending on type, entrance aspect ratio is 30 : 80 or 200 : 80 and where diverging angle is 4° or 8°; full lines in Fig. 5.3 show results of calculations by using the theory of two-dimentional equation. As seen here, results of experiments for diffuser of inlet aspect ratio of 2.5 are nearly the same as those of two-dimentional calculation.

For aspect ratio smaller than 0.4, however, experimental values differ greatly from calculated values. For small aspect ratio, two-dimentional calculation should be modified by considering effects of three-dimentionality.

3. Theoretical consideration

When aspect ratio becomes small, it is considered that side wall friction has the effect of retarding boundary layer flow on diverging wall. In order to estimate the effect, momentum balance was considered for flow in a cross-section of the diffuser, where we assume that the flow is nearly two-dimentional. However, the effect of side wall friction is too small to explain the discrepancy between theory and experiment in Fig. 5.3.

Consequently, we know that the effect of side wall friction is small when the flow is nearly two-dimentional.

Next, we consider a effect of non-twodimentionality of flow on thicknesses of boundary layer. When boundary layer flow in the diffuser is not two-dimentional, that is to say, when stream-lines on a plane parallel to wall are not parallel, as shown in Fig. 5.4 and in Eq. (4.40), the momentum equation is

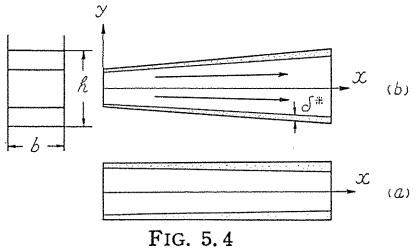

FIG. 5.4

$$\frac{d\theta}{dx}+\frac{\theta}{U}\frac{dU}{dx}(2+H)=\frac{\tau_0}{\rho U^2}-\psi_0\theta. \quad (5.1)$$

Value of this additional term $\psi_0=(d\alpha/dz)_{z=0}$ depends on boundary layer on side

wall, on divergency of diffuser and on secondary flow.

If there is no secondary flow in a cross-section of a diffuser, streamlines on a plane near and parallel to the side wall diverge uniformly, as in Fig. 5.4 (b) and streamlines near the diverging wall converge slightly because of thickening of boundary layer on side wall, as in Fig. 5.4 (a). Thus the additional term in Eq. (5.1) for boundary layer on diverging wall and side wall can be expressed respectively as

$$\theta\psi_0 = -\frac{2\theta}{(b-2\delta_s^*)}\frac{d\delta_s^*}{dx}, \qquad \theta_s\psi_0 = \frac{\theta_s}{(h-2\delta^*)}\left(\frac{dH}{dx}-2\frac{d\delta^*}{dx}\right) \tag{5.2}$$

where subscript s denotes values for boundary layer on side wall. The effects of these aditional terms of Eq. (5.2) is to decrease thickness on side wall, and increase slightly thicknesses on diverging wall.

Values of momentum thickness calculated by using Eq. (5.2) are compared with experimental values on wall center in diffuser of small aspect ratio, as shown in Fig. 5.5. As seen here, results of calculation by using Eq. (5.2) are closer to the experimental results than those by two-dimentional calculation.

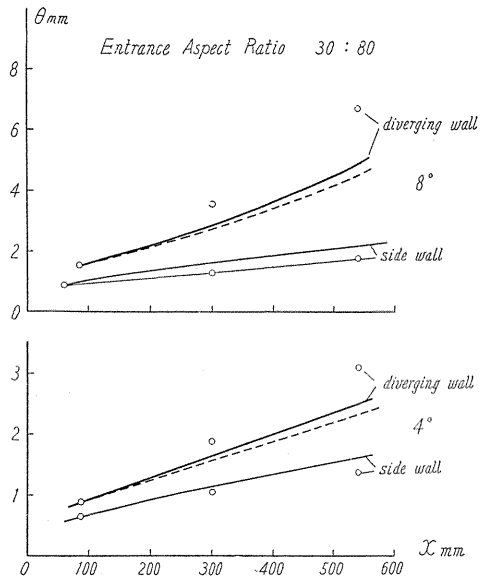

FIG. 5.5

However, there still remains a difference between results of calculation and experiment. Here, we recognized that experimental values at short side of wall (diverging wall in Fig. 5.5) is greater than the calculated values, but the experimental values at long side of wall (side wall in Fig. 5.5) is smaller than the calculated value.

Experimental displacement thicknesses at center of walls are compared with those of cross-sectional average values which are obtained from experiments on pressure distribution, as shown in Fig. (5.6). Here, we recognized also that layer thicknesses at the center of short side of wall are markedly greater than the average values but that layer thicknesses at center of long side of wall are not greater, are rather even smaller, than the average.

These discrepancies will depend on secondary flow in a cross-section, because Eq. (5.2) disregards effect of secondary flow in a cross-section. If secondary flow occurs in a diffuser, value of $\psi_0\theta$ in Eq. (5.1) will vary across the wall and differ from the mean value of Eq. (5.3). Therefore local value of layer thickness is considered to be affected by the secondary flow.

4. Effect of secondary flow

Experiments on velocity contour lines in a cross-section (Fig. 5.7) show that there are secondary flows in the cross-section, as seen in Fig. 5.8. The same

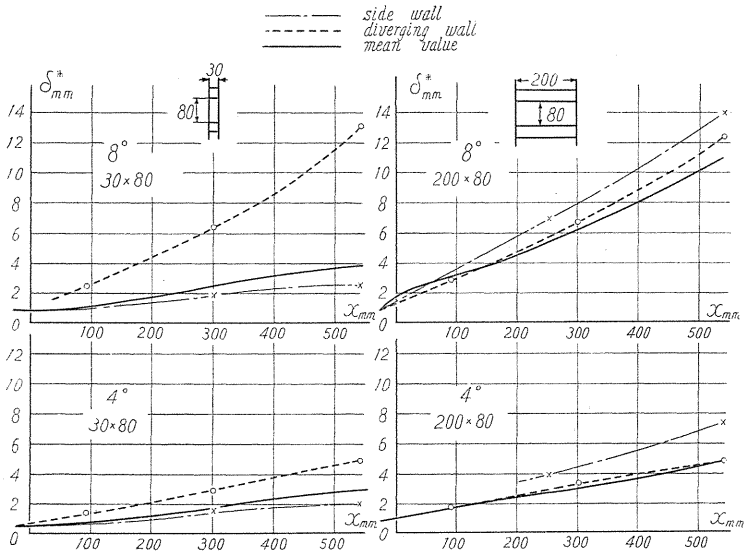

FIG. 5.6

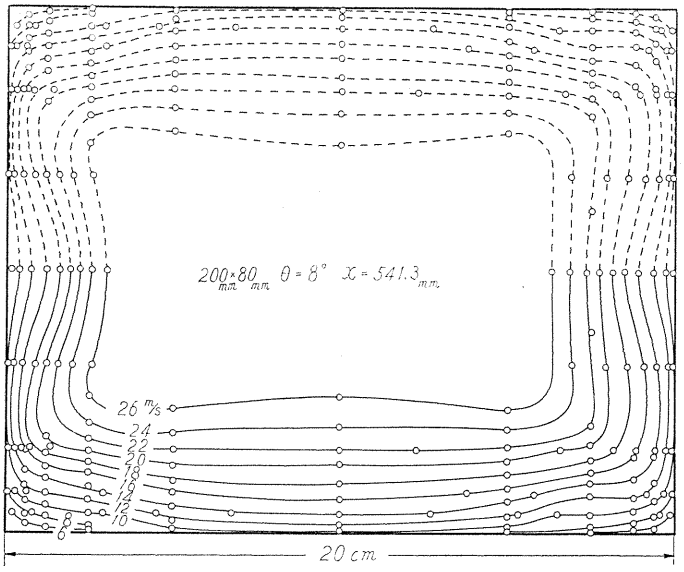

FIG. 5.7 (*a*)

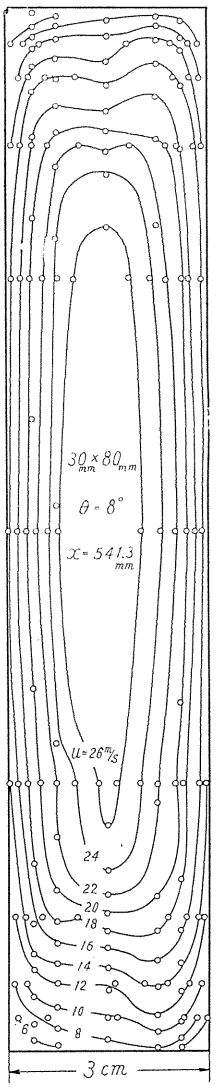

FIG. 5.7 (*b*)

results as ours were given in Nikuradse's experiments[41] for rectangular parallel pipe although he did not use diverging pipe, as we did.

Fig. 5.8 shows that layer thicknesses at center of the short side of wall is greatly increased by the secondary flow, but that layer thicknesses at center of the longer side of wall is not increased, or may even be slightly decreased. These conditions qualitatively agree with our experiments described above.

Consequently, the effect of secondary flow can be considered as follows: The

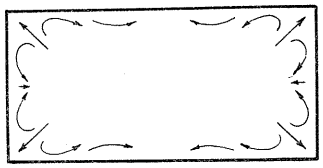

FIG. 5.8

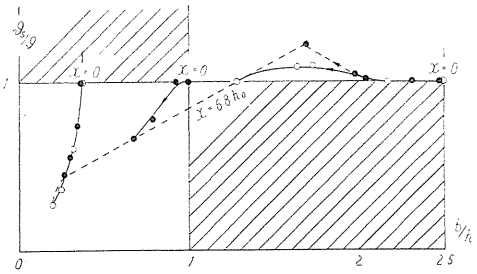

FIG. 5.9

ratio of local thickness on side wall center to that on diverging wall θ_s/θ becomes smaller or larger than 1 according by as the aspect ratio is smaller or larger than 1. Therefore by combinding the secondary flow effect with effect of Eq. (5.2) which shows that the ratio θ_s/θ is generally smaller than 1, we see that the ratio θ_s/θ becomes very much smaller than 1 when the aspect ratio is smaller than 1, but the value θ_s/θ is only slightly larger than 1 when the aspect ratio is larger than 1. These conditions are in good agreement qualitatively with our experiments as shown in Fig. 5.9.

5. Cross-sectional average value

The average layer thickness in a cross-section is more important than the local thickness when considering the pressure performance of diffusers prior to flow separation because the average thickness determines pressure in each cross-section.

Although the secondary flow changes layer thickness locally in a cross-section, when the average of local thickness is taken in the cross-section, the secondary flow effect will be decreased by cancelling out local change.

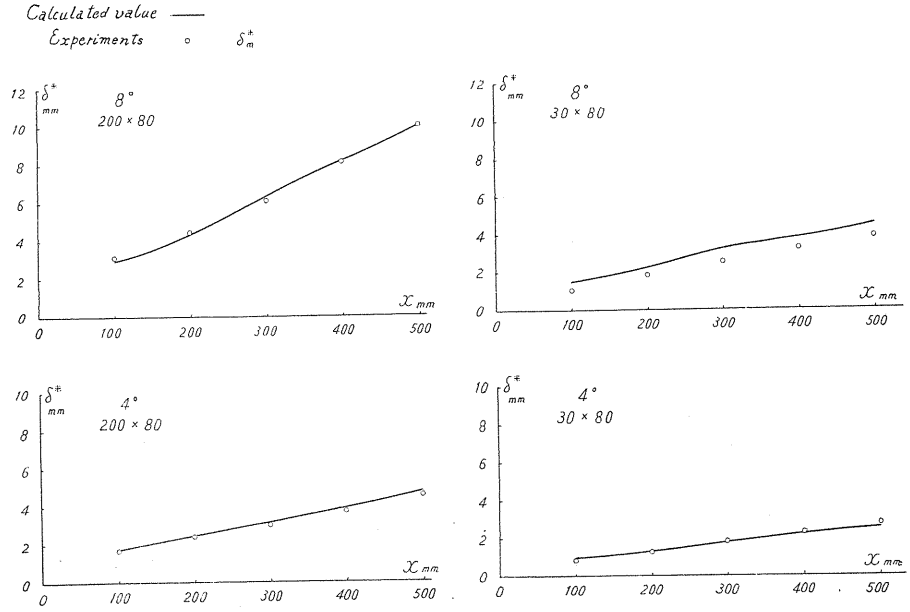

FIG. 5.10

Cross-sectional average values of displacement thickness are calculated by using calculated value of θ with Eq. (5.1) and the value of mean profile parameter $H=1.35$. Comparing these values with experimental values, as shown in Fig. 5.10, the agreement is good.

Consequently we can calculate pressure performance in rectangular diffuser before flow separation, disregarding the secondary flow effect.

6. Conclusion

Experiments are carried out to examine the effect of width on the two-dimentionality of boundary flow in rectangular diffusers having constant width.

When the aspect ratio of this rectangular section *i.e.* the ratio of distance between two parallel side walls to distance between two diverging walls is larger than 2, flow on diverging wall is nearly two-dimentional and can be calculated by two-dimentional theory.

When aspect ratio is smaller than 1, local thicknesses at center of diverging wall is greatly increased by the effect of secondary flow as well as by that of side wall boundary layers, but layer thickness on side wall are decreased by these effects.

However, disregarding these effects, the important cross-sectional average thickness can be calculated even for diffusers of aspect ratio smaller than 1.

Chapter VI. Test Application of Formulae and Theories

1. Effect of boundary layer thickness on flow in diffuser

In designing diffusers, it is important to estimate the separation point of flow as well as to decide the thickness of boundary layer.

Thickness of boundary layer decides behavior of flow before separation in diffuser as well as diffuser performance. Separation of flow from the wall results in loss of energy and increased vibration. By using our theory on flow in diffuser and our experimental results thus far given, thickness of boundary layer, velocity profile and separation point can be calculated with more accuracy.

In this section we give examples of calculations showing how the thickness of boundary layer at the entrance affects the flow in the diffuser.

When pressure along the flow has been previously determined, momentum thickness of boundary layer and parameter of velocity profile can be given by step-by-step calculations of the two simultaneous equations (4.24) and (4.28) for two-dimentional diffuser or (4.32) and (4.28) for axially symmetrical diffuser. Separation point is given when the value of H is 1.8. Fig. 6.1 shows results of calculation when the potential flow in a two-dimentional diffuser has a diverging angle of 8°. Fig. 6.1 (a) is parameter H *vs.* x/h (x: distance from entrance along flow, h: width of entrance) and Fig. 6.1 (b) is momentum thickness $\frac{\theta}{h_0}R_0^{1/4}$ *vs.* x/h_0 both for various boundary layer thickness at the entrance (for $\theta_0/h_0=0$, 1, 2%) and both for $U_0h_0/\nu=10^5$.

As the layer thickness at the entrance increases, the separation point approaches the entrance (Fig. 6.1 (a)), although distribution of boundary layer thickness (non-dimentional thickness $\frac{\theta}{h_0}R_0^{1/4}$) is quickly affected by entrance thickness (Fig. 6.1 (b)).

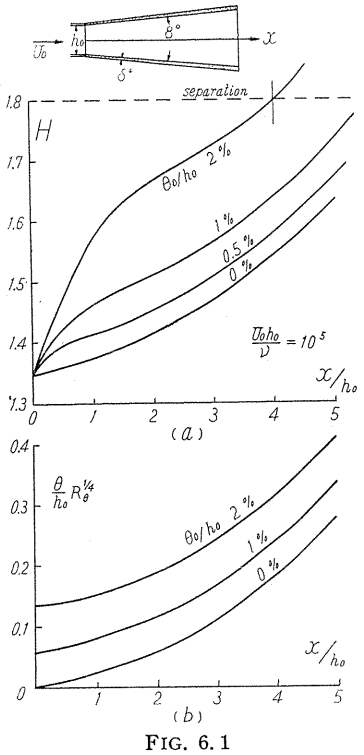

FIG. 6.1

In these calculation we have assumed pressure to be constant in each cross-section of diffuser and, by use of Bernoulli's theorem velocity outside boundary layer U is assumed constant in each cross-section. This assumption is verified by our experiments except for some diffuser types, *i.e.* where in the cross-section close to the entrance pressure gradient on the wall becomes greater than near the axis. In this case it is easier for the separation point to come near the entrance because of greater pressure gradient.

Figs. 6.2 and 6.3 are results of calculations when the diverging angle is 10°. Comparing Fig. 6.2 with Fig. 6.1 we see that the separation points in Fig. 6.2 (diverging angle of 10°) comes nearer to the entrance ($x/h_0 < 5$) than those of Fig. 6.1 (diverging angle of 8°).

Fig. 6.3 shows the effect of Reynolds number at entrance $U_0 h_0/\nu$ (U_0: velocity at the entrance) on the thickness of layer in each cross-section. The greater the Reynolds number becomes, the thinner the boundary layer grows.

In Fig. 6.3 (a), dotted lines give the distribution of displacement thickness δ^*/h_0 which increase greatly along the flow. Because the potential flow diverges straightly ahead and because the cross-sectional area of diffuser should be greater than that of

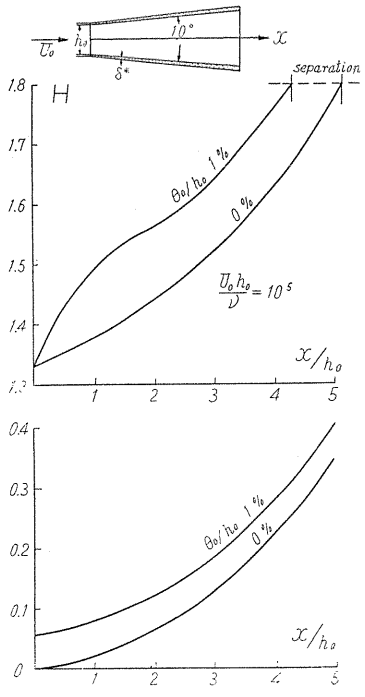

FIG. 6.2

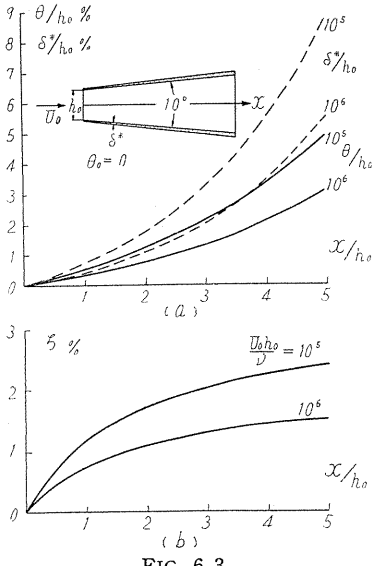

FIG. 6.3

potential flow by the displacement thickness, thus the shape of diffuser differs somewhat in to a trumpet-like form.

When the shape of diffuser is previously known, calculations of flow becomes somewhat more complicated than when pressure p is known, because velocity outside boundary layer U should be calculated from both the values of displacement thickness and form of diffuser by using Eq. (1.4).

Therefore, calculations should be carried out by solving three simultaneous equations concerned with θ, U and $H=\delta^*/\theta$ instead of two equations concerned with θ and H.

Fig. 6.4 compares results of these calculations of flow in a diffuser of rectangular cross-section (full line) where the distance between two parallel walls is kept constant and two other walls diverge at an angle of 10°, with the flow in Fig. 6.3 (dotted line) where the potential flow diverges at an angle of 10°, both conditions for the same thickness of boundary layer at entrance and for the same Reynolds number. In this case (full line) separation of flow does not occurs as easily when compared with the previous cases, because the boundary layer thickness suppresses the main flow and reduces pressure rise and occurance of separation.

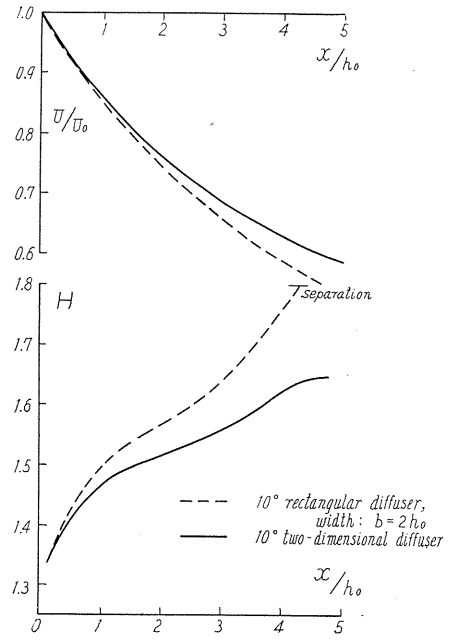

FIG. 6.4

From the above, we can see that the boundary layer thickness at the entrance usually has the effect of easy separation, but this is not true when the boundary layer thickness suppresses the main flow.

2. Comparison of calculated separation point with experimental results[42]

a) Experimental results

There have been many experimental studies made on the efficiency of diffusers and loss of energy through diverging flow but few experimental results have been published on the phenomenon of flow and its state of separation.

Experiments on the separation of flow in a 20° conical diffuser are carried out by this author and others.[43] Here we describe the experiments and compare experimental separation points with theoretically calculated separation points of flow.

The 20° conical diffuser used on this investigation is shown in Fig. 6.5. This diffuser can be separated into two parts divided in a plane including the center axis of the diffuser. The diffuser is connected to the approach pipe which, in turn, is connected to a contraction pipe and a blower. By lengthening the approach pipe length l from 2.25 D_0 to 24.5 D_0 (D_0: entrance diameter), the thickness of boundary layer at entrance to the diffuser is increased.

For visual observation of separation of flow in the diffuser, short length of

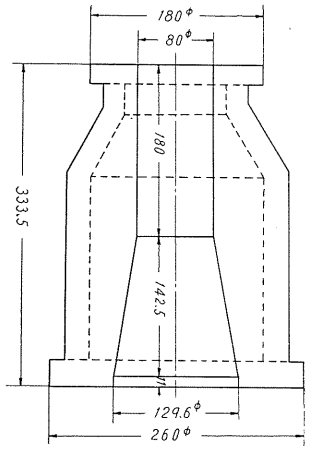

FIG. 6.5

silk thread are knotted all along two steel wires, stretched across the outlet section of the diffuser. Fig. 6.6 represents four views, each differing in approach pipe length and Reynolds number at entrance $\overline{U}_0 D_0/\nu$ ($\overline{U}$: mean velocity). All these views show that a reverse flow occurs near the wall.

In these experiments there is a considerable fluctuation of flow such as pressure oscillating 4–8% of its mean head. The correlation of velocity between points in the outlet section of the diffuser is measured by using two hot-wire anemometers. Fig. 6.7 gives examples of correlation measurements. When the two points come close together in the same side of the same section (Fig. 6.7 first image, left), the correlation is good. On the other hand, when the two points are on opposite sides of that section, (Fig. 6.7 last image, right) there is a reverse correlation between the velocities of the two points.

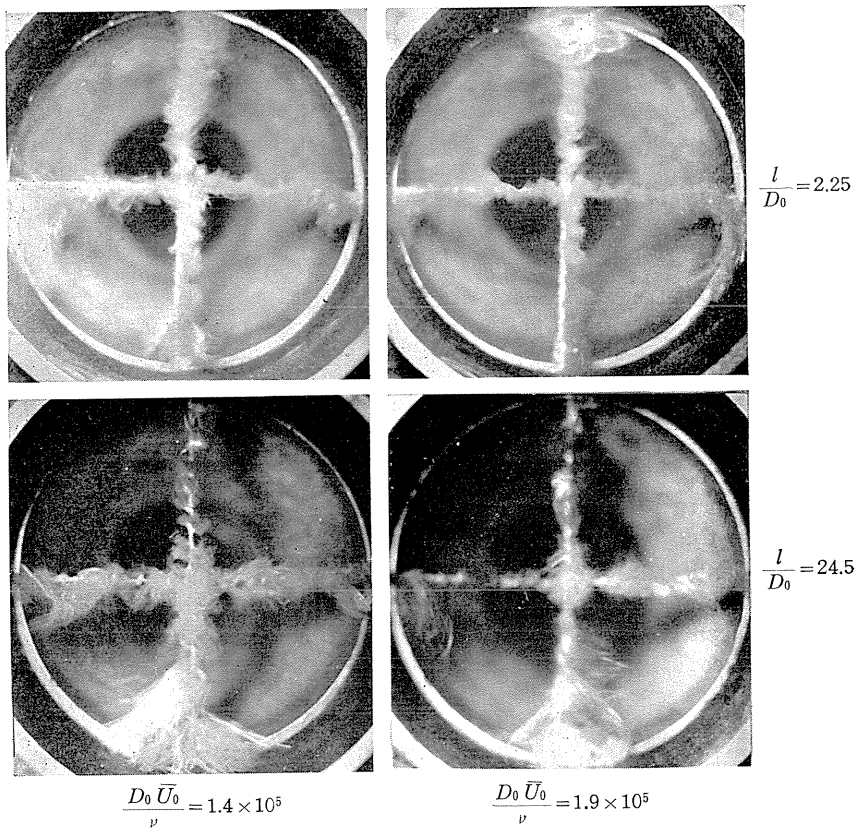

FIG. 6.6

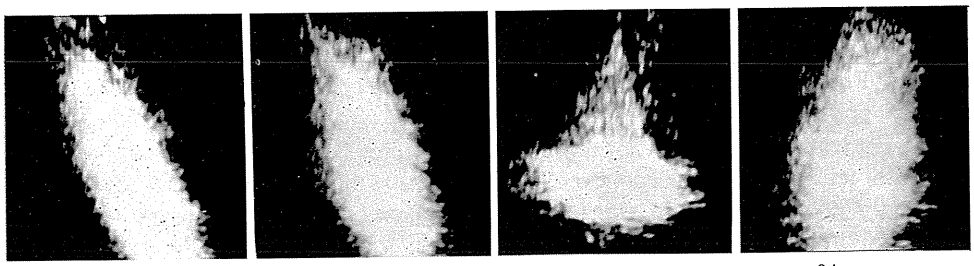

FIG. 6.7

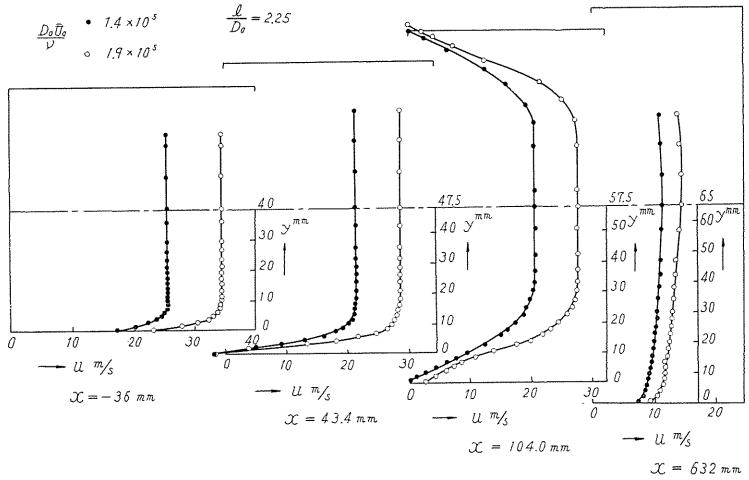

FIG. 6.8

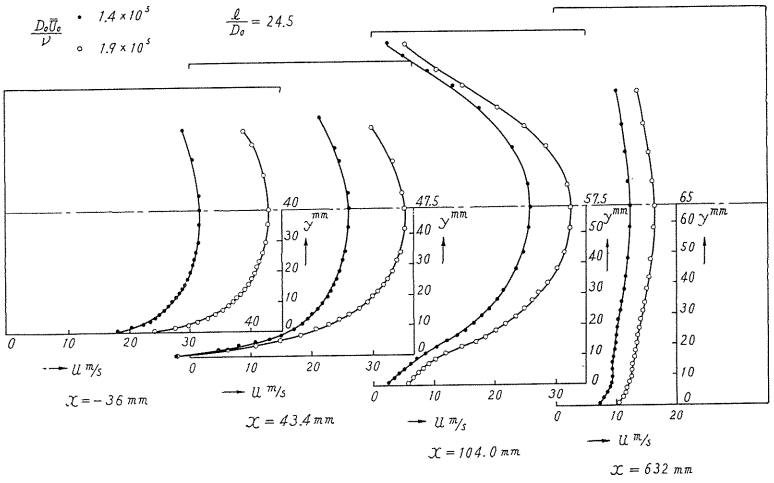

FIG. 6.9

Figs. 6.8 and 6.9 show the velocity distribution at stages before entering, while within and after leaving the diffuser. Here the length of approach pipe is 2.25 D for Fig. 6.8 and 24.5 D for Fig. 6.9 respectively, and here $\overline{U}_0 D_0/\nu$ is 1.4×10^5 for black ponts and 1.9×10^5 for white points.

The central part of velocity profiles in both stages before entering ($x=-36$ mm) and while within the diffuser ($x=43.4$ mm, $x=104$ mm) are similar; reverse flow occurs only near the wall in stages $x=43.4$ mm and 104 mm. The values of parameter H of these velocity profiles are 2.3-3.2. In the section of the tail pipe where pressure is maximum ($x=632$ mm), the value of parameter H returns to the value at the entrance 1.25-1.3.

Pressure distribution shown in Fig. 6.10 and Fig. 6.11 when l/D_0 is 2.25 and 24.5 respectively.

The chain lines here represent pressure distribution for frictionless fluid.

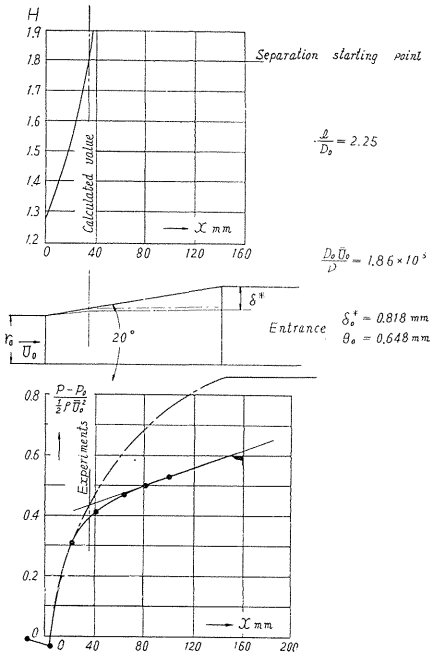

FIG. 6.10

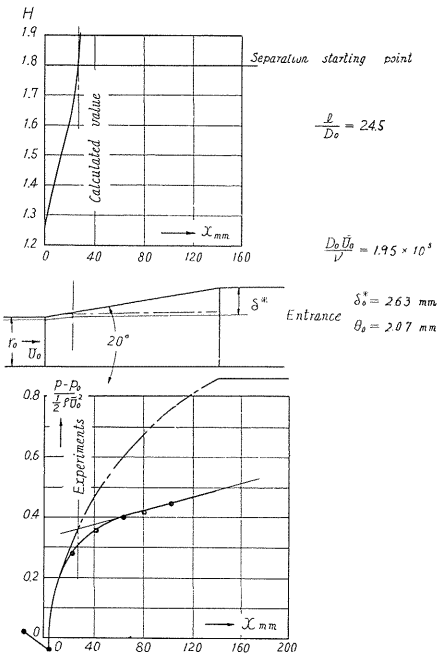

FIG. 6.11

b) Determination of starting point of separation of flow

It is difficult to decide the exact starting point of flow separation in these experiments because of the presense of velocity pulsation. We can calculate displacement thickness δ^* by experiments on both velocity and pressure distributions. By plotting δ^* distribution along the wall of the diffuser, we can see that the thickness increases greatly at a point where the main flow forms as a jet at an angle of divergence of less than 4° and is not influenced by the wall of the diffuser (see Fig. 6.10 and 6.11), this point can be assumed to be the separation starting point.

c) Comparison of calculated separation point with experimental results

In our method of calculating turbulet boundary layer in diffuser, the equation of parameter H is given as follows:

$$\theta R_0^{1/4} dH/dx = -\alpha\Gamma - \beta$$

where

$$R_0 = U\theta/\nu \qquad \Gamma = \frac{\theta}{U}\frac{dU}{dx}R_\theta^{1/4}$$

and α and β are functions of only H as shown in Fig. 4.11, IV. In this method it is assumed that the separation of flow starts when the value of parameter H is 1.8.

By using this equation with both the equation of momentum thickness which is

$$\frac{d\theta}{dx} + \theta\left[(H+2)\frac{1}{U}\frac{dU}{dx} + \frac{1}{r_0}\frac{dr_0}{dx}\right] = \frac{\tau_0}{\rho U^2}$$

and the equation of velocity just outside the boundary layer

$$\frac{U}{\overline{U}} = \left(1 - 2\frac{\delta^*}{r_0}\right)$$

where $\overline{U}$ is mean velocity in a cross-section, we can calculate the separation starting point.

These results for two different inlet pipe lengths are shown in Figs. 6.10 and 6.11.

A comparison of the position of the separation point with the experimental results, shows good agreement, as seen in these figures, which proves the increased accuracy of our theory.

Acknowledgement

The author expresses his appreciation to Professor Emeritus Dr. K. Shogenji of Nagoya University for his encouragement thourghout this research, and to Professor Emeritus Dr. S. Suzuki of Tokyo University for his guidance and to Professor Dr. T. Koga for his valuable advice.

The author acknowledges his debt to Prof. Dr. T. Yamamoto and members of Hydraulic Laboratory of Nagoya University for their help in carrying out this research.

Thanks go to Mr. K. Suzuki, Mr. E. Tanaka and Mr. Y. Sugiyama for their assistance in some of these experiments.

References

1) Gibson, A. H., Hydraulics and its application. 5th edition p. 92, Constable and Co.
2) Andres, K., Versuche über die Umsetzung von Wassergeschwingigkeit im Druck. Z. VDI, Bd. **54**, Nr. 38-39 (1910).
3) Lyon, G. E., Flow in conical draft tubes of varying angles. Trans. of American Soc. Mech. Engrs., 43 (1931).

4) Peters, H., Energieumsetzung in Querschnittserweiterungen bei verschiedenen Zulaufbedingungen. Ing.-Archiv, Bd. **2**, Heft 1 (1931).
5) Vüller, H., Ausnutzung der kinetischen Austrittsenergie der Luft bei Ventilatoren mittels Diffusoren. Z. VDI, Bd. **77**, Nr. 31 (1933).
6) Shogenji, K., Memoirs of the Faculty of Engineering, Kyushu Imperial University, Vol. **4**, 2 (1927).
7) Fujimoto, B., The experimental results of diverging flow. Bulletin of the Engineering Institute Kyoto University, Vol. **2**, p. 18 (1951).
8) Hochschild, H., Experiments on flow in diverging and converging channels. Forschung., Ver. Deut. Ing., Heft 114 (1919).
9) Kröner, R., Versuche über Stömungen in stark erweiterten Kanalen. Forschung., VDI, Heft 222 (1919).
10) Dönch, F., Divergente und Konvergente Strömungen mit kleinen Öffnungswinkeln. Forschung., VDI, Heft 292 (1926).
11) Nikuradse, J., Untersuchungen über die Strömungen des Wassers in konvergenten und divergenten Kanalen. Forschung., VDI, Heft 289 (1929).
12) Gruschwitz, E., Die turbulente Reibungsschicht in ebener Strömung mit Druckabfall und Druckanstieg. Ing.-Archiv, Bd. **2**, p. 321 (1931).
13) Buri, A., Eine Berechnungsgrundlage für die turbulente Grenzschicht bei beschleunigter und verzögerter Strömung. Dissertation, Zürich (1931).
14) Kehl, A., Über konvergente und divergente turbulente Reibungsschichten. Ing.-Archiv, Bd. **12**, p. 293 (1943).
15) Doenhoff, A. E. and Tetervin, T., Determination of General relations for the behavior of turbulent boundary layers. N.A.C.A., Tech. Report No. 772 (1943).
16) Garner, H. C., The development of turbulent boundary layers. A.R.C., R and M, No. 2133 (1944).
17) Rotta, J., Beitrag zur Berechunung der turbulente Grenzschichten. Ing.-Archiv, Bd. **19**, p. 31 (1951).
18) Truckenbrodt, E., Zur angenäherten Berechnung der laminaren und turbulenten Grenzschicht fur ebene und rotationsymmetrische Strömung. Ing.-Archiv, Bd. **20**, Heft 4 (1952).
19) Fujimoto, B., Practical methods of calculating the boundary layer. Technical Reports of the Engineering Research Institute, Kyoto University, Vol. **2**, No. 2, Report No. 7 (1952).
20) Schuh, H., On calculation incompressible turbulent boundary layers with arbitrary pressure distribution. Kungl, Tekniska Hogskolan, Technical Notes 41 (1941).
21) Patterson, G. N., Modern Diffuser Design. Aircraft Engineering, Vol. **10**, p. 267 (1938). see 4.
22) Wieghardt, K. and Tillmann, W., Deutsche Luftfahrtforschung. Untersuchungen und Mitteilungen, Bericht Nr. 6617 (1944).
23) Durand, W. F., Aerodynamic Theory, Vol. **III**, p. 108, Springer.
24) Furuya, Y., Turbulent boundary layers in diverging flow; Universal velocity distribution near the wall. Trans. of Japan Soc. of Mech. Engrs., Vol. **9**, No. 81 (1955).
25) Stanton, T. E. and others, On the condition at the boundary of a fluid in turbulent motion. Proc. Roy. Soc., London A, **97**, p. 413 (1920).
26) Furuya, Y., The velocity distribution in turbulent boundary layer in diverging flow. Trans. of Japan Soc. Mech Engrs., Vol. **19**, No. 81 (1953).
27) Prandtl, L., Uber die ausgebildete Turbulenz. Z.A.M.M., **5**, 136 (1925) and Proc. 2nd Int. Cong. Appl. Mech., Zurich, p. 62 (1926).
28) Ludwieg, H. and Tillmann, W., Untersuchungen über die wandschubspannung in turbulenten Reibungsschichten. Ing.-Archiv, Bd. **17**, p. 288 (1949).
29) Sandborn, V. A., Preliminary experimental investigation of low-speed turbulent boundary Layers in adverse pressure gradients. N.A.C.A., Tech. Notes 3031 (1953).
30) Furuya, Y., Turbulent boundary layer in diverging flow; a new method for estimating turbulent boundary layers. Trans. of Japan Soc. Mech. Engrs., Vol. **21**, No. 121 (1956).

31) Clauser, F. H., Turbulent boundary layers in adverse pressure gradients. Jr. Aero. Sci., Vol. **21**, p. 91 (1954).
32) Coles, D., The law of the wake in the turbulent boundary layer. G.A.L.C.I.T., Rep. Dec. 20, 1955.
33) Schultz-Grunow, F., Neues widerstandsgestz fur glatten Platten. Luftfahrtforschung, Bd. **17**, p. 239 (1940).
34) Prandtl, L., Über den Reibungswiderstand strömender Luft. Ergebnisse d. Aerod. Versuchsanst. zu Göttingen IV Lieferg. (1930).
35) Kármán, T., Mechanische Ähnlichkeit und Turbulenz. Nachrichten Ges. Wiss. or Schlichting, H. Grenzschicht Theorie. p. 355. G. Braun Karlsruhe.
36) Schlichting, H., Grenzschicht Theorie. p. 394. G. Braun Karlsruhe.
37) Hama, R., Boundary-layer characteristics for smooth and rough surfaces. Annual Meeting, Naval Architects and Marine Engr. Nov. 1954.
38) Millikan, C. B., The boundary layer and skin friction for a figure of revolution. Trans. American Soc. Mech. Engrs., Vol. **54**, No. 2, p. 29 (1932).
39) Schubauer, G. B. and Klebanoff, P. S., Investigation of separation of the turbulent boundary layer. N.A.C.A., Tech. Notes 2133 (1950).
40) Furuya, Y. and Sugiyama, Y., On the boundary layer thickness in rectangular diffuser. Read at the general meeting of Japan Soc. Mech. Engrs. on April, 1957.
41) Schiller, L., Handbuch der Experimental Physik, IV, Teil 4, p. 15.
42) Furuya, Y. and Suzuki, K., Experiments on the efficiency of conical diffuser. Trans. Japan Soc. Mech. Engrs., Vol. **23**, No. 125 (1957).
43) Mr. Suzuki, K. and Mr. Tanaka, E.